

# **AIM: A User-friendly GUI Workflow program for Isotherm Fitting, Mixture Prediction, Isosteric Heat of Adsorption Estimation, and Breakthrough Simulation**

Muhammad Hassan<sup>a</sup>, Sunghyun Yoon<sup>a</sup>, Yu Chen<sup>a</sup>, Pilseok Kim<sup>b</sup>, Hongryeol Yun<sup>c</sup>, Hyuk Taek Kwon<sup>d</sup>, Youn-Sang Bae<sup>e</sup>, Chung-Yul Yoo<sup>f</sup>, Dong-Yeun Koh<sup>g</sup>, Chang-Seop Hong<sup>c</sup>, Ki-Bong Lee<sup>b</sup>, Yongchul G. Chung<sup>a,h\*</sup>

<sup>a</sup> School of Chemical Engineering, Pusan National University, Busan, 46241, Republic of Korea

<sup>b</sup> Department of Chemical and Biological Engineering, Korea University, 145 Anam-ro, Seongbuk-gu, Seoul 02841, Republic of Korea

<sup>c</sup> Department of Chemistry, Korea University, Seoul 02841, Republic of Korea

<sup>d</sup> Department of Chemical Engineering, Pukyong National University, 45 Yongso-ro, Nam-gu, Busan, 48513, Republic of Korea

<sup>e</sup> Department of Chemical and Biomolecular Engineering, Yonsei University, 50 Yonsei-ro, Seodaemun-gu, Seoul, 03722, Republic of Korea

*<sup>f</sup> Department of Energy Systems Research and Chemistry, Ajou University, 206, World Cup-ro, Yeongtong-gu, Suwon 16499, Republic of Korea*

*<sup>g</sup> Department of Chemical and Biomolecular Engineering (BK-21 Plus), Korea Advanced Institute of Science and Technology (KAIST), Daejeon 34141, Republic of Korea*

*<sup>h</sup> Graduate School of Data Science, Pusan National University, Busan, 46241, Republic of Korea*

\*Corresponding author. E-mail: [drygchung@gmail.com](mailto:drygchung@gmail.com) (Y.G. Chung)

## **Abstract**

Adsorption breakthrough modeling often requires complex software environments and scripting, limiting accessibility for many practitioners. We present AIM, a MATLAB-based graphical user interface (GUI) application that streamlines fixed-bed adsorption analysis through an integrated workflow for isotherm fitting, heat of adsorption estimation, mixture prediction, and multicomponent breakthrough simulations. AIM's intuitive GUI requires no coding and supports a broad isotherm library (e.g., Langmuir, Toth, Dubinin-Astakhov, Structural-Transition-Adsorption). It also enables non-isothermal breakthrough simulations with axial dispersion. Case studies, such as Xe/Kr breakthrough curves in SBMOF-1, closely match the results from other software applications, such as RUPTURA. Mixture predictions can be done using the Ideal Adsorbed Solution Theory (IAST) and Extended Langmuir models, while isosteric heats are derived from Clausius-Clapeyron or Virial equations. Users can export detailed column and outlet profiles (e.g., composition, temperature) in multiple formats, enhancing reproducibility and data sharing among practitioners.

## *Keywords:*

Open-source GUI software, adsorption isotherm fitting, fixed bed adsorption breakthrough modelling, mixture isotherm prediction

**Program summary**

Program title: AIM

Developer's repository link: <https://github.com/mtap-research/AIM>

Licensing provision: GPL-2.0

Programming language: MATLAB

Operating system: Windows, Mac, Linux

Nature of problem: Adsorption isotherm modelling; prediction of mixture gas adsorption and breakthrough curves for fixed bed system using ideal adsorption solution theory (IAST) or extended model mixture adsorption model

Solution method: Adsorption isotherm fitting; isosteric heat of adsorption via Clausius-Clapeyron or Virial equation; IAST nonlinear equation solution; solution of dynamic fixed bed material and energy balances using finite volume method (FVM)

## 1. Introduction

Adsorption-based separation processes are considered an energy-efficient method for separating and purifying gases. These processes exploit the selective adsorption of one component over another on porous materials [1]. The industrial applications of adsorption processes include hydrogen gas purification, air separation, hydrocarbon separation or air dehumidification [2]. The performance of adsorbent materials can be evaluated based on their primary factors (i.e. adsorbent textural properties, equilibrium isotherms); however, the performance evaluation incorporating secondary factors, such as heat and mass transfer resistances, particle size, and pressure drop, is important in practical implementation of the adsorption material [3–7].

For fixed bed systems, breakthrough experiments can be conducted to evaluate the performance of adsorbent under dynamic conditions [8,9]. In a typical breakthrough experiment, a column packed with a bed of adsorbent is pressurized and purged with a carrier gas, which is usually inert. The gaseous mixture is then introduced at the column inlet, and the concentrations of the different components are recorded at the outlet. The adsorption of components in a gaseous mixture occurs as the mixture passes over the adsorbent. The adsorption process continues until the point when the adsorbent becomes saturated. Once the adsorbent becomes saturated, the adsorbates ‘breakthrough’ the column and the concentration profile of the adsorbate in the effluent as a function of time is termed as breakthrough curve. Breakthrough curves, which show how gas concentrations change over time at the outlet of an adsorbent column, are often used to characterize dynamic separation performance of adsorbent materials.

Dynamic adsorption characteristics of adsorbent materials can be characterized based on the breakthrough simulations. Breakthrough simulations have been used to quantify and rank the separation potential of various types of adsorbent materials for CO<sub>2</sub> capture [10,11], Xe/Kr separation [12,13], and hydrocarbon separations [14,15]. There have been several performance metrics developed based on the breakthrough results such as the breakthrough time of preferentially adsorbing gas [16] and separation potential [17]. The breakthrough time of the more adsorbing gas is the total duration after which the more adsorbing gas exits from the adsorber column. These metrics correlate well with the productivity of the fixed bed. The separation potential is the maximum amount of the less adsorbing gas which can be recovered from the adsorber column and is based on the mixture adsorption loadings at the fixed bed inlet conditions.

The mixture adsorption loadings are typically estimated based on the Ideal Adsorbed Solution Theory (IAST) developed by Myers and Prausnitz [18]. The model assumes negligible axial dispersion and mass transfer resistance which leads to sharper and nearly vertical breakthrough curves [17,19]. However, in many cases the condition of negligible axial dispersion is not achieved due to low gas velocities and increased molecular diffusivity [20]. Similarly, larger particle size and low values of intra-particle diffusivities can lead to non-negligible mass transfer resistance causing significant deviations from the adsorption equilibrium [21]. In such cases, a high-fidelity breakthrough simulation accounting for axial dispersion and mass transfer, and other adsorber parameters are necessary for accurate performance evaluation of adsorbent materials.

Several commercial simulation software packages are available for breakthrough simulations, such as Aspen Adsorption, gPROMS Adsorption Library, ProSim Dynamic Adsorption Column, and AVEVA's Process Simulation Adsorption Library. These software applications are often used in literature to understand and predict the dynamic separation behavior of adsorbent materials, but the lack of standardized computational workflow and transparency of implemented methods for isotherm fitting, mixture prediction, and availability of breakthrough simulation parameters hampers the reproducibility of simulation results [22]. Moreover, many of these simulations are carried out in commercial software packages which makes it difficult to share workflow and raw data with other researchers without the software license. To remedy the situation, there has been some effort in developing open-source software tools for adsorption applications, such as pyIAST [23], IAST ++ [24], and pyGAPS [25] (isotherm fitting and mixture adsorption), RUPTURA [26] (isotherm fitting, mixture adsorption, and breakthrough simulation), pyAPEP [27], and ToPSail [28] (isotherm fitting, mixture adsorption prediction, and pressure swing adsorption cycle simulation). However, these software applications require the preparation of programming script or text input file, which may limit accessibility for practitioners.

We present a MATLAB-based graphical user interface (GUI) software package called 'AIM'. AIM provides an integrated workflow for adsorption isotherm fitting at single and multiple temperatures, isosteric heat of adsorption estimation, mixture isotherm prediction, and multicomponent adsorption breakthrough simulations. Unlike existing tools such as pyIAST and RUPTURA, which require scripting expertise or access to Linux terminal, AIM offers a seamless, GUI-driven application for isotherm fitting, isosteric heat of adsorption estimation, and

breakthrough simulation. AIM has four modules – IsoFit, HeatFit, MixPred, and BreakLab as shown in **Figure 1**. IsoFit and HeatFit are modules for isotherm fitting for single and multiple temperatures, respectively. Both IsoFit and HeatFit incorporate different isotherm models such as Langmuir, Langmuir–Freundlich, Quadratic, and Brunauer–Emmett–Teller (BET), and others. MixPred module can be used to calculate mixture adsorption loadings based on the IAST and extended dual-site Langmuir (EDSL) models. BreakLab module can simulate isothermal/non-isothermal breakthrough process for up to five components and produce temperature and concentration profiles in the column and at the outlet. The integrated workflow using AIM modules is shown in **Scheme 1**. The output files from IsoFit and HeatFit can be conveniently used to predict mixture adsorption using MixPred or to simulate breakthrough process via BreakLab. GUI features of individual modules streamline the user experience by systematically carrying out isotherm fitting and breakthrough simulations with the user-defined inputs.

This article is structured as follows. First, we describe the file format and general guidelines for preparing IsoFit and HeatFit modules data input file. We then explain the different modules available in AIM along with the underlying models (**Section 3-6**). In **Section 7** we will provide the details of numerical methods employed for isotherm fitting and breakthrough simulations. The results for different case studies conducted using AIM modules are provided in **Section 8** to demonstrate the performance of AIM. The codes and compiled GUI application software can be accessed from GitHub (<https://github.com/mtap-research/AIM>).

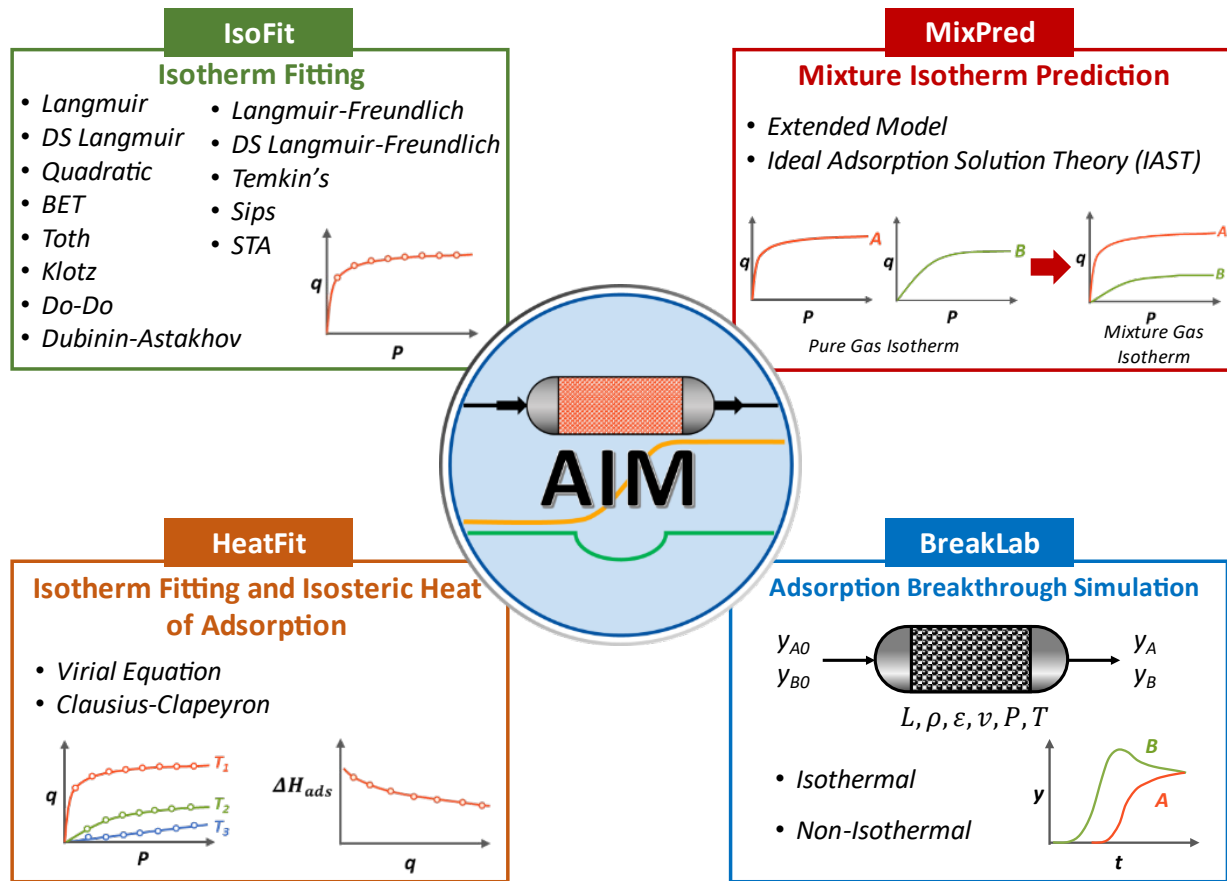
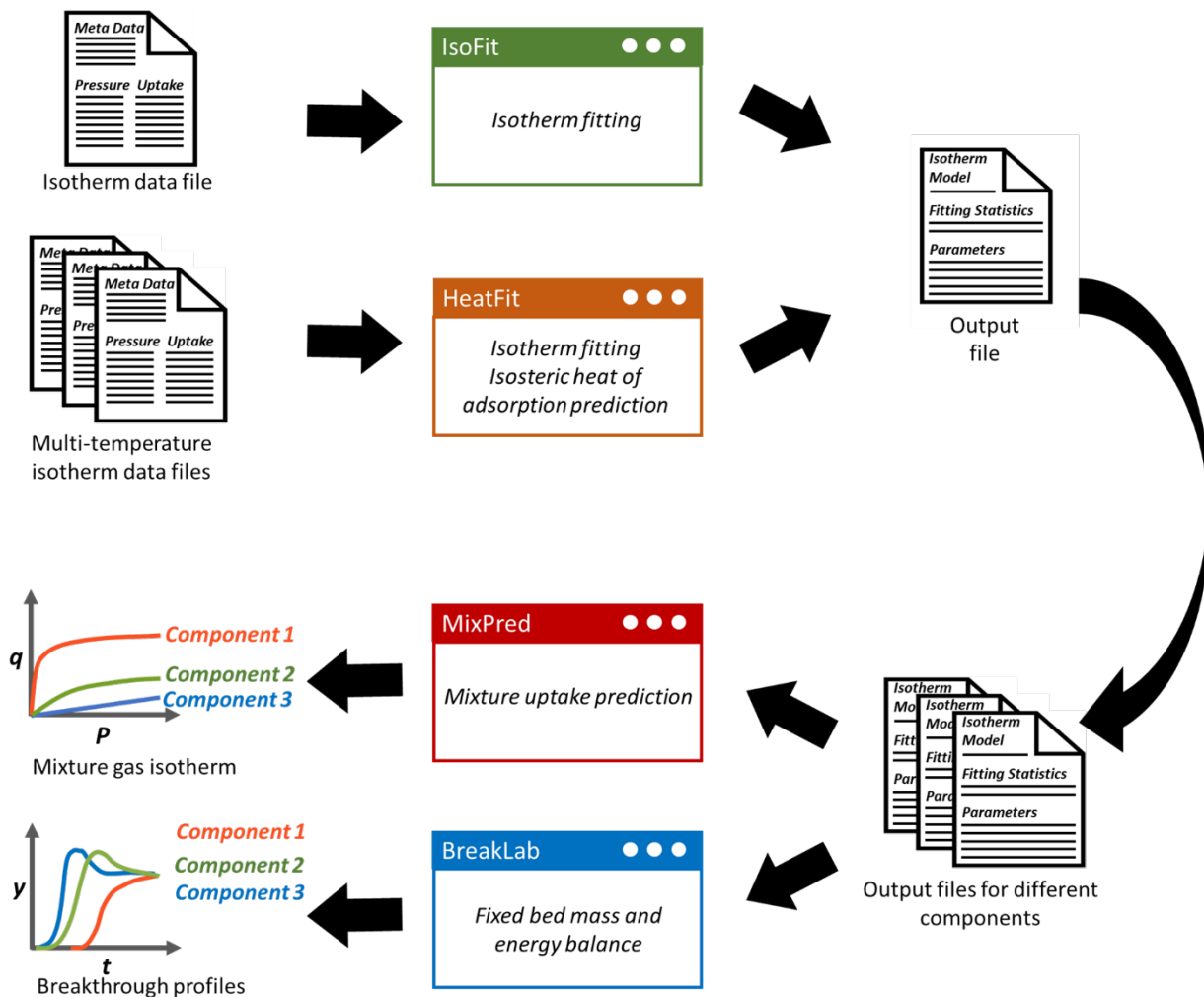


**Fig. 1.** Overview of AIM modules. **IsoFit** for isotherm fitting, **HeatFit** for multiple temperature isotherm fitting and isosteric heat of adsorption prediction, **MixPred** for mixture isotherm predictions using the IAST and EDSL models, and **BreakLab** for multicomponent isothermal and non-isothermal breakthrough simulations



**Scheme 1.** Integrated workflow for isotherm fitting, mixture isotherm prediction and breakthrough simulation using AIM modules. IsoFit and HeatFit modules can read and fit the single and multiple temperature isotherm data for isotherm fitting, respectively. The fitting results from IsoFit and HeatFit can be saved in an output file, which contains the isotherm model, fitted parameters, and fitting statistics. The output file from HeatFit also contains the predicted isosteric heat of adsorption value. The fitted isotherm model and the parameters can be directly loaded into MixPred and BreakLab modules by importing the output files for various components. MixPred mixture model uses the loaded isotherm model and parameters to calculate mixture adsorption isotherm. BreakLab uses the isotherm model and parameters to dynamically evaluate the mixture uptakes based on the fixed bed process conditions



## 2. Input and output data files

AIM modules IsoFit and HeatFit read isotherm data from input file and generate output file containing isotherm fitting results. Both the input and output files have a well-defined and human-readable format to ensure accessibility to users with diverse backgrounds. In this section, we outline the supported file formats, required keywords, and guidelines to facilitate isotherm data file preparation.

### 2.1. Input file description

IsoFit and HeatFit can import isotherm data from

- General input data files in the following formats: \*.csv, \*.txt, \*.xlsx, \*.dat.
- Adsorption Information Format (AIF) [29].

The general input data file contains tabular data with columns corresponding to pressure and adsorption uptake values. Additionally, the user can specify the meta information in the input file such as temperature value and units of pressure, adsorption uptake, and temperature. A typical input file for IsoFit and HeatFit modules is shown in **Figure 2**.

```
#units_pressure Pa
#units_loading mol/kg
#sat_pressure 2022
#temperature 298
#units_temperature K
72.4957      0.1400
161.1015     0.2451
229.5697     0.3326
318.1756     0.4201
394.6988     0.5427
503.4423     0.7177
579.9656     0.9103
```

**Fig. 2.** An example of input data file for IsoFit and HeatFit modules. The header of the input data file contains meta information about the isotherm data. The meta information is followed by tabular data with two columns representing pressure and uptake values

We recommend following the guidelines below while preparing the generic input data file

- The first column of the isotherm data should contain pressure values, and the second column should contain gas adsorption uptake (adsorption loading) values.
- The columns should be separated either by a single tab, whitespace, or comma.
- The meta information should be specified at the beginning of the file followed by isotherm data.
- The meta information requires specific tags which are listed in **Table 1**. The module will only search for and parse the tags listed in **Table 1**. Any additional tags will be ignored.
- The tag names and values should be specified in the following manner:  
Tag\_1\_Name Tag\_1\_Value  
Tag\_2\_Name Tag\_2\_Value  
...
- In the case of importing data from a spreadsheet (\*.xlsx), please specify the data in the first sheet.
- If the AIF file contains both adsorption and desorption data, only the adsorption data will be read. In case isotherm fitting using desorption data is required, please use a separate input file.
- The temperature value is read only in HeatFit module. IsoFit ignores the temperature value.

In addition to isotherm data, IsoFit also requires saturation/total pressure ( $P_0$ ) to calculate the relative pressure in the case when user choose either 'Auto' or Dubinin-Astakhov, Klotz, and Do-Do models. The  $P_0$  can be specified via one of the following methods:

- In the meta information of the isotherm data file using the tag listed in **Table 1**.
- In the app itself using the  $P_0$  entry field.
- By directly specifying the relative pressure values instead of pressure values in the isotherm data file. In this case, specify  $P_0 = 1$  in the  $P_0$  entry field.

**Table 1.** Tags name for specifying meta information in the input data files

<b>Description</b>	<b>General input data file</b>	<b>AIF</b>
Pressure unit	#units_pressure	_units_pressure
Gas adsorption uptake unit	#units_loading	_units_loading
Saturation/total Pressure	#sat_pressure	_adsorp_p0
Temperature value	#temperature	_exptl_temperature
Temperature unit	#units_temperature	_units_temperature

## 2.2. Output file description

IsoFit and HeatFit generate an output file containing the isotherm model name, fitted parameters, and fitting statistics. Fitting statistics include Root Mean Square Error (RMSE) and  $r^2$  value. The output file from HeatFit also contains reference temperature used for fitting and fitted isosteric heat of adsorption values. The output file uses custom extension '\*.bliso' to facilitate integrated workflow within AIM modules. However, the file itself is human-readable and can be opened with any text editor such as Notepad, WordPad etc. The fitted isotherm parameters in the output file can be directly loaded in MixPred and BreakLab modules for mixture adsorption prediction and breakthrough simulation, respectively. The user is advised not to modify the extension and keywords in the output file, as this can cause issues in isotherm parameter loading. **Figure 3** shows an example output file from IsoFit.

```
*****
*****IsoFit ISOTHERM FITTING RESULTS*****
*****
Isotherm Model: DS-Langmuir

RMSE:    0.004575
r^2:     1.000000

Parameters
q_sat_1   2.263656
b_1       1.811334e-05
q_sat_2   1.753061
b_2       5.744321e-07
*****
```

**Fig. 3.** A typical output file from IsoFit module showing the fitted isotherm model, fitting statistics, and the resulting isotherm parameters

### 3. IsoFit – Isotherm fitting at single temperature

For a given adsorbent and adsorbate at constant temperature, the relationship between the pressure of the adsorbate and the equilibrium loading in adsorbent material is expressed as an adsorption isotherm. Adsorption isotherms can be obtained from atomistic simulation, such as grand canonical Monte Carlo (GCMC) simulation, or from experiments. The data can be then fitted into different isotherm models which expresses the mathematical relationship between adsorption loading, pressure, and temperature. IsoFit is a module that can load the isotherm data and fit isotherm models. **Figure 4** shows the GUI window of IsoFit. The isotherm data imported by user is displayed in the tabular format and is also plotted. The user can choose different isotherm models for fitting, and the module displays the fitted isotherm model curve, and reports the fitted parameters in the Output panel. The Isotherm Fitting Settings window allows users to define initial guesses, as well as lower and upper bounds for the fitting parameters. Additionally, the user can test multiple initial guesses using multistart feature, which enables IsoFit to use different random initial guesses for isotherm fitting and select the best results. **Table 2** also summarizes the isotherm model expressions and the respective fitting parameters. We describe details of the isotherm models implemented in IsoFit in subsequent section.

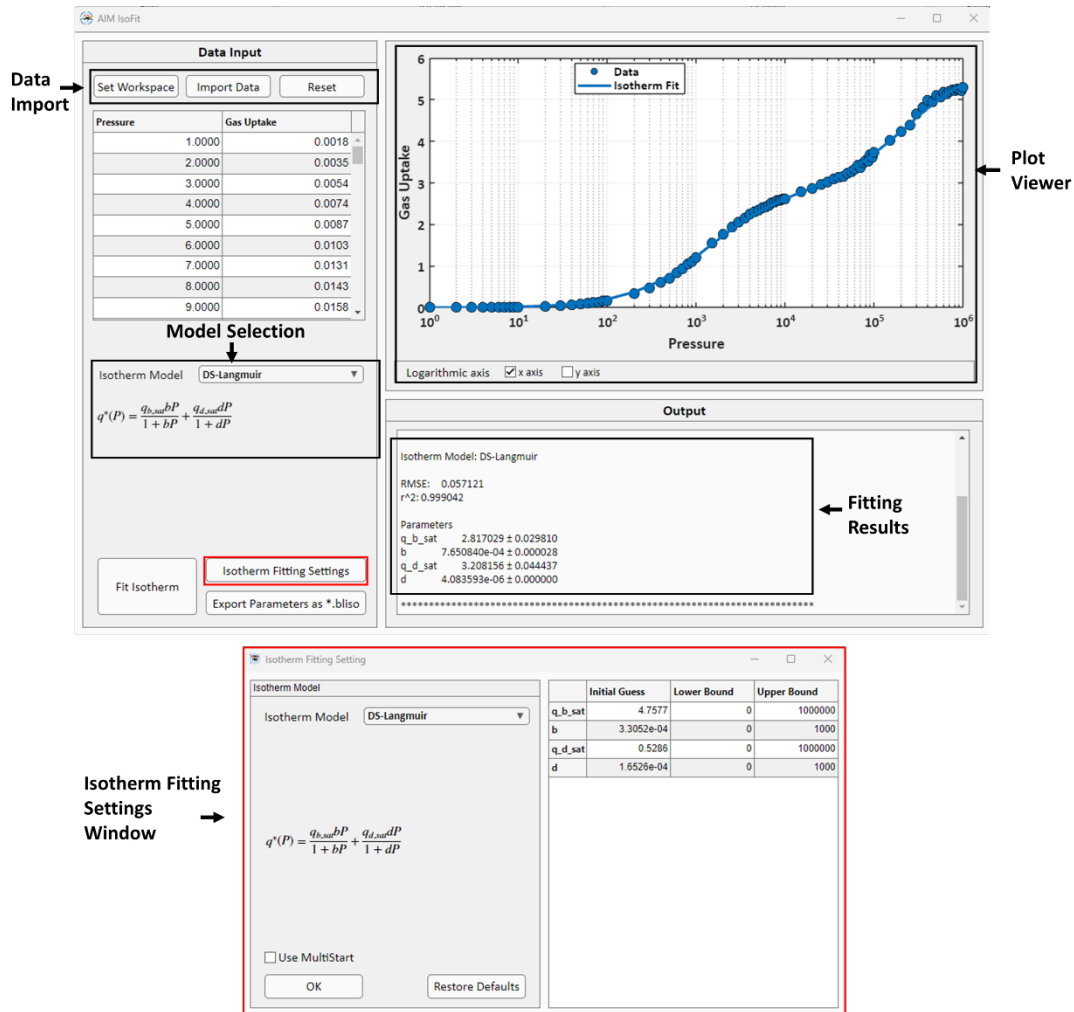


**Fig. 4.** IsoFit GUI with main isotherm fitting interface and Isotherm Fitting Settings dialogue box. **Data Input:** access to loading isotherm data and isotherm model selection for fitting. **Plot Viewer:** displays the fitted isotherm model curve and isotherm data. **Output:** numerical output of fitted parameters and the fitting statistics. **Isotherm Fitting Settings:** access to the initialization of the fitting procedure using user-defined initial guesses and upper and lower bounds for isotherm model parameters

**Table 2.** Isotherm models available in IsoFit

<b>Isotherm Models</b>	<b>Expression</b>	<b>Parameters</b>
Langmuir	$q^* = \frac{q_{sat}bP}{1 + bP}$	$q_{sat}, b$
Dual-site Langmuir	$q^* = \frac{q_{sat,1}b_1P}{1 + b_1P} + \frac{q_{sat,2}b_2P}{1 + b_2P}$	$q_{sat,1}, b_1, q_{sat,2}, b_2$
Langmuir-Freundlich	$q^* = \frac{q_{sat}bP^n}{1 + bP^n}$	$q_{sat}, b, n$
Dual-site Langmuir-Freundlich	$q^* = \frac{q_{sat,1}b_1P^{n_1}}{1 + b_1P^{n_1}} + \frac{q_{sat,2}b_2P^{n_2}}{1 + b_2P^{n_2}}$	$q_{sat,1}, b_1, n_1, q_{sat,2}, b_2, n_2$
Quadratic	$q^* = q_{sat} \left( \frac{bP + cP^2}{1 + bP + cP^2} \right)$	$q_{sat}, b, c$
Temkin	$q^* = q_{sat} \left( \frac{bP}{1 + bP} \right) + q_{sat}\theta \left( \frac{bP}{1 + bP} \right)^2 \left( \frac{bP}{1 + bP} - 1 \right)$	$q_{sat}, b, \theta$
BET	$q^* = \frac{q_{sat}bP}{(1 - cP)(1 - cP + bP)}$	$q_{sat}, b, c$
Sips	$q^* = \frac{q_{sat}(bP)^{\frac{1}{n}}}{1 + (bP)^{\frac{1}{n}}}$	$q_{sat}, b, n$
Toth	$q^* = \frac{qbP}{(1 + (bP)^n)^{\frac{1}{n}}}$	$q_{sat}, b, n$
Structural-Transition-Adsorption	$y(P) = \left( \frac{1 + b_{NP}P_{tr}}{1 + b_{NP}P} \right)^{q_{NP}} \left( \frac{1 + b_{LP}P_{tr}}{1 + b_{LP}P} \right)^{q_{LP}},$ $\sigma(P) = \frac{y^s}{1 + y^s},$ $q^* = (1 - \sigma) \left( \frac{q_{NP,sat}b_{NP}P}{1 + b_{NP}P} \right) + \sigma \left( \frac{q_{LP,sat}b_{LP}P}{1 + b_{LP}P} \right)$	$q_{NP,sat}, b_{NP}, q_{LP,sat}, b_{LP}, s, P_{tr}$
Dubinin-Astakhov	$x = \frac{P}{P_0}, \quad q^*(x) = q_{sat} e^{-\left(\frac{1}{K} \ln \frac{1}{x}\right)^n}$	$q_{sat}, K, n$
Klotz	$x = \frac{P}{P_0}, \quad s = Kx,$ $q^* = q_{sat} \frac{Cs\{1 - (1 + n)s^n + ns^{n+1}\}}{(1 - s)1 + (C - 1)s - Cs^{n+1}}$	$q_{sat}, K, C, n$
Do-Do	$x = \frac{P}{P_0},$ $q^* = q_{sat} f \frac{K_1 x 1 - (1 + \beta)x^\beta + \beta x^{\beta+1}}{(1 - x)1 + (K_1 - 1)x - K_1 x^{\beta+1}} + (1 - f) \frac{K_2 x^\alpha}{1 + K_2 x^\alpha}$	$q_{sat}, f, K_1, K_2, \alpha, \beta$

### 3.1. Langmuir isotherm model

The Langmuir isotherm model is based on the monolayer coverage of the adsorption sites with homogeneous interaction sites and first proposed by Langmuir [30]. The isotherm equation is given as

$$q^* = \frac{q_{sat}bP}{1 + bP} \quad (1)$$

where  $q_{sat}$  is the monolayer saturation capacity of adsorbent and  $b$  is the Langmuir constant that describes the affinity of the adsorbate and adsorbent, and  $P$  is the system pressure. The Langmuir isotherm given by equation (1) is only valid when the adsorbent surface is energetically homogenous.

### 3.2. Dual-site Langmuir isotherm model

Graham [31] proposed a dual-site Langmuir isotherm model to account for the heterogeneity of an adsorbent surface by incorporating two distinct adsorption binding sites. The dual-site Langmuir model is given as

$$q^* = \frac{q_{sat,1}b_1P}{1 + b_1P} + \frac{q_{sat,2}b_2P}{1 + b_2P} \quad (2)$$

where  $q_{sat,1}$ ,  $q_{sat,2}$  are the monolayer saturation capacities, and  $b_1$ ,  $b_2$  are the Langmuir constants corresponding to site 1 and 2, respectively.

### 3.3. Langmuir-Freundlich isotherm model

The Langmuir-Freundlich isotherm model was proposed by Sips [32] to account for the heterogenous nature of adsorbent surface. The model was later utilized to explain dissociative chemisorption of hydrocarbon on activated charcoal [33]. The isotherm model equation is given as,

$$q^* = \frac{q_{sat}bP^n}{1 + bP^n} \quad (3)$$



where  $q_{sat}$  is the monolayer saturation capacity,  $b$  is the Langmuir constant, and  $n$  is the factor accounting for adsorbent surface heterogeneity. The model reduces to the Langmuir isotherm model when  $n$  is 1.

### 3.4. Dual-site Langmuir-Freundlich isotherm model

The Langmuir-Freundlich isotherm model can be improved to better represent a heterogeneous adsorbent surface by incorporating an additional adsorption site. The resulting isotherm model is referred to as the dual-site Langmuir-Freundlich isotherm. The model equation is given as

$$q^* = \frac{q_{sat,1}b_1P^{n_1}}{1 + b_1P^{n_1}} + \frac{q_{sat,2}b_2P^{n_2}}{1 + b_2P^{n_2}} \quad (4)$$

where  $q_{sat,1}$ ,  $q_{sat,2}$  are the monolayer saturation capacities;  $b_1$ ,  $b_2$  are the Langmuir constants, and  $n_1$ ,  $n_2$  are the surface heterogeneity factors corresponding to site 1 and 2, respectively.

### 3.5. Quadratic isotherm model

Statistical thermodynamics proposes that the general form of an isotherm model is the ratio of two polynomials of identical degrees [34].

$$q^* = q_{sat} \left( \frac{bP + 2cP^2 + 3dP^3 + \dots}{1 + bP + cP^2 + dP^3 + \dots} \right) \quad (5)$$

In the literature, the second order expansion of the above isotherm model is often employed referred to as quadratic isotherm model expressed as [35]:

$$q^* = q_{sat} \left( \frac{bP + 2cP^2}{1 + bP + cP^2} \right) \quad (6)$$

The quadratic isotherm model exhibits an inflection point: the loading is convex at low pressures (anti-Langmuir adsorption) but gradually changes concavity as the adsorbent saturates [36] (Langmuir adsorption), forming an S-shape.

### 3.6. Temkin isotherm model

Temkin adsorption isotherm model, similar to Langmuir model, assumes homogeneity of adsorption sites, but it also incorporates the adsorbate-adsorbate interactions based on the linear dependence of the heat of adsorption on coverage. IsoFit incorporates the asymptotic approximation of the Temkin isotherm model derived by Simon *et al.* [37] using the mean-field argument. The isotherm model is given as:

$$q^* = q_{sat} \left( \frac{bP}{1 + bP} \right) + q_{sat} \theta \left( \frac{bP}{1 + bP} \right)^2 \left( \frac{bP}{1 + bP} - 1 \right) \quad (7)$$

The parameter  $\theta$  represents the strength of the adsorbate–adsorbate interactions. Values of  $\theta < 0$  imply attraction, while  $\theta > 0$  implies repulsion.

### 3.7. BET isotherm model

Brunauer, Emmett, and Teller (BET) isotherm model is a generalization of the Langmuir model to multilayer adsorption [38]. The BET model assumes that the adsorption sites are energetically homogenous, but the adsorbate molecules could form multiple layers without limit. The isotherm model is given as:

$$q^* = \frac{q_{sat} bP}{(1 - cP)(1 - cP + bP)} \quad (8)$$

where  $b$  and  $c$  are the Langmuir constants for the first layer of adsorbate on the bare surface of the adsorbent and for the subsequent layers on top of the first layer, respectively.

### 3.8. Sips isotherm model

Sips isotherm model is a combination of the Langmuir and Freundlich isotherms and is given as [32,39]

$$q^* = q_{sat} \frac{(bP)^{\frac{1}{n}}}{1 + (bP)^{\frac{1}{n}}} \quad (9)$$

where the parameter  $n$  represents the adsorbent surface heterogeneity. When  $n$  is 1, Sips model reduces to the Langmuir model, indicating that the adsorbent has homogenous binding sites. Both Sips (equation 9) and Langmuir-Freundlich (equation 3) isotherms are combinations of Langmuir and Freundlich models and are mathematically equivalent. We can recover equation 3 from equation 9 by setting  $b_{LF} = (b_{Sips})^{1/n_{Sips}}$ , and  $n_{LF} = 1/n_{Sips}$ , where  $b_{LF}$ ,  $b_{Sips}$  and  $n_{LF}$ ,  $n_{Sips}$  are the Langmuir constants and surface heterogeneity constants for Langmuir-Freundlich and Sips models, respectively. Since both isotherm models are widely used in literature, we have implemented both models in IsoFit.

### 3.9. Toth isotherm model

Toth isotherm model is another empirical modification of Langmuir model [40,41], and given as:

$$q^* = q_{sat} \frac{bP}{[1 + (bP)^n]^{\frac{1}{n}}} \quad (10)$$

where the parameter  $n$  characterize the system heterogeneity and is usually less than 1. For the cases where  $n = 1$ , the model reduces to Langmuir model. The Toth equation satisfies both low-pressure and high-pressure limiting conditions. At low pressures the model reduces to Henry's law with Henry coefficient of  $q_{sat}b$ , while at high pressures the model yields a finite saturation limit equal to  $q_{sat}$ .

### 3.10. Structural transition adsorption isotherm model

Flexible MOFs undergo adsorption-induced structural transition referred to as “gate-opening” or “breathing”, resulting in an S-shaped isotherms. Structural transition adsorption (STA) model is a

statistically derived isotherm model that can be used to model adsorption isotherm of flexible metal-organic framework (MOFs) [42]. STA equation has six parameters which are  $q_{NP,sat}$ ,  $b_{NP}$ ,  $q_{LP,sat}$ ,  $b_{LP}$ ,  $s$ , and  $P_{tr}$ . The STA model is expressed as [42],

$$q^*(P) = (1 - \sigma) \left( \frac{q_{NP,sat} b_{NP} P}{1 + b_{NP} P} \right) + \sigma \left( \frac{q_{LP,sat} b_{LP} P}{1 + b_{LP} P} \right) \quad (11)$$

where subscripts  $NP$  and  $LP$  stand for narrow-pore and large-pore, representing the state of adsorbent before and after the adsorption-induced transition, respectively.  $q_{NP}$ ,  $b_{NP}$ , and  $q_{LP}$ ,  $b_{LP}$  are the Langmuir isotherm model parameters for the  $NP$  and  $LP$  regions, respectively.  $\sigma$  is the S-shaped function which smoothly connects the  $NP$  and  $LP$  isotherm curves and is expressed as,

$$\sigma(P) = \frac{y^s}{1 + y^s} \quad (12)$$

$$y(P) = \left( \frac{1 + b_{NP} P_{tr}}{1 + b_{NP} P} \right)^{q_{NP}} \left( \frac{1 + b_{LP} P_{tr}}{1 + b_{LP} P} \right)^{q_{LP}}, \quad (13)$$

where  $s$  is the parameter representing the shape of adsorption-induced structural transition. A high value of  $s$  indicate more abrupt and steeper transition between the  $NP$  and  $LP$  regions.  $P_{tr}$  is the threshold or transition pressure, i.e. the pressure where the adsorbent structural transition occurs.

### 3.11. Dubinin-Astakhov isotherm model

Dubinin-Astakhov (DA) isotherm model has been applied to describe S-shaped (type V) adsorption isotherms which appear in flexible MOFs and water adsorption cases. DA model was developed based on the assumption that adsorption on microporous adsorbents is governed by a micropore filling [43]. The model equation is [44],

$$q^*(x) = q_{sat} e^{-\left(\frac{RT}{\epsilon} \times \ln \frac{1}{x}\right)^n} \quad (14)$$

$$x = \frac{P}{P_0} \quad (15)$$

where  $P_0$  is the saturation pressure of the adsorbate,  $q_{sat}$  is the saturation capacity of adsorbent when  $P = P_0$ ,  $R$  is the general gas constant,  $T$  is the given temperature,  $\epsilon$  is the characteristic free energy of adsorption, and  $n$  is the parameter accounting for surface heterogeneity. IsoFit uses the following form of DA model for isotherm fitting [45],

$$q^*(x) = q_{sat} e^{-\left(\frac{1}{K} \times \ln \frac{1}{x}\right)^n} \quad (16)$$

where  $K$  is the lumped parameter representing the characteristic free energy of adsorption and temperature.

### 3.12. Klotz isotherm model

Klotz isotherm model is to model an S-shaped isotherm. The model is based on the concept of Klotz originally developed for protein interaction with small molecules [46]. The Klotz isotherm model considers multi-layer adsorption process and assumes formation of adsorbate clusters which are in equilibrium with one another. The Klotz equation has four parameters which are  $q_{sat}$ ,  $K$ ,  $C$ , and  $n$ . The Klotz equation reads as [47]

$$q^*(s) = q_{sat} \frac{Cs\{1 - (1 + n)s^n + ns^{n+1}\}}{(1 - s)1 + (C - 1)s - Cs^{n+1}} \quad (17)$$

$$s = Kx \quad (18)$$

$$x = P/P_0 \quad (19)$$

where  $P_0$  is the saturation pressure of the adsorbate,  $q_{sat}$  is the saturation capacity of adsorbent,  $n$  is the maximal association number representing the degree of adsorbate cluster formation (i.e. number of adsorbate layers in cluster),  $K$  is the clustering constant describing adsorbate-adsorbate interaction, and  $C$  is the ratio of the affinity of the adsorbate and adsorbent and clustering constant  $K$ . A high value of  $C$  indicates strong adsorbate-adsorbent interactions.

### 3.13. Do-Do isotherm model

Do-Do isotherm model mathematically describes the type IV isotherm, which is characterized by an initial formation of a few adsorption layers at lower pressures, followed by pore filling [48]. Do-Do model was originally developed for explaining adsorption and desorption of water on

activated carbon [49]. The model assumes that the adsorption process initiates with formation and growth of water clusters via hydrogen bonding around the functional sites. These functional sites correspond to the location of functional groups. Micropore adsorption proceeds only after some critical size of these functional site bound cluster is achieved [49,50]. Do-Do model has six parameters which are  $q_{sat}$ ,  $f$ ,  $K_1$ ,  $\alpha$ ,  $\beta$ , and  $K_2$ . The model equation is given as [50],

$$q^*(x) = q_{sat} \left( f \frac{K_1 \sum_{n=1}^{\beta} n x^n}{1 + K_1 \sum_{n=1}^{\beta} x^n} + (1-f) \frac{K_2 \sum_{n=\alpha+1}^{\beta} x^n}{K_2 \sum_{n=\alpha+1}^{\beta} x^n + \sum_{n=\alpha=1}^{\beta} x^{n-\alpha}} \right) \quad (20)$$

$$x = P/P_0 \quad (21)$$

where  $P_0$  is the saturation pressure of the adsorbate,  $q_{sat}$  is the saturation capacity of adsorbent,  $f$  is the fraction of functional sites,  $K_1$  is the clustering constant at the functional site,  $\beta$  is the maximal association number representing the degree of adsorbate cluster formation at the functional site,  $\alpha$  is the critical size for micropore adsorption, and  $K_2$  is the interaction constant between the water molecules in the micropore. In IsoFit, we use the following form of the model equation derived by Buttersack [47] using series summation given as

$$q^*(x) = q_{sat} \left( f \frac{K_1 x \{1 - (1 + \beta)x^{\beta} + \beta x^{\beta+1}\}}{(1-x)\{1 + (K_1 - 1)x - K_1 x^{\beta+1}\}} + (1-f) \frac{K_2 x^{\alpha}}{1 + K_2 x^{\alpha}} \right); \beta > \alpha \quad (22)$$

$$x = P/P_0 \quad (23)$$

#### 4. HeatFit – Isotherm fitting at multiple temperature

In the previous section, we discussed the isotherm models which describe the adsorption loading and pressure corresponding at a single temperature. The adsorption loadings at different temperatures are related to the isosteric heat of adsorption, which can be useful for modeling non-isothermal adsorber system. The isosteric heat of adsorption is a specific case of the heat of adsorption that is determined at constant adsorption loading (i.e., fixed coverage). Alternatively, the isosteric heat of adsorption can be obtained by fitting multiple temperature isotherm data for the isotherm model via the Clausius-Clapeyron equation, which relates adsorption equilibrium at different temperatures. The isosteric heat of adsorption as a function of coverage can be useful in

understanding how strongly molecules are bound to different coverages. Detailed discussion of the isosteric heat of adsorption can be found in the literature [51,52].

HeatFit is a module which estimates the isosteric heat of adsorption based on user-provided isotherm data. HeatFit supports two different models (Clausius-Clapeyron and Virial) to obtain the isosteric heat of adsorption. **Figure 5** shows the GUI window of HeatFit. To run the HeatFit module, the user needs to first load multi-temperature isotherm data, which will be displayed in the tabular format and plotted. Note that the user is required to provide the temperature values for a given isotherm data. Isotherm fitting procedure is carried out for the chosen isotherm model. Once the isotherm fitting is complete, HeatFit plots the fitted isotherm model curve, and reports the fitted parameters in the Output panel. The users can define initial guesses, as well as lower and upper bounds for the fitting parameters in the Isotherm Fitting Setting window. Additionally, the user can test multiple initial guesses using multistart features, which enables HeatFit to generate different random initial guesses for isotherm fitting and select the best results. The resulting isotherm parameters can be saved in several different file formats.

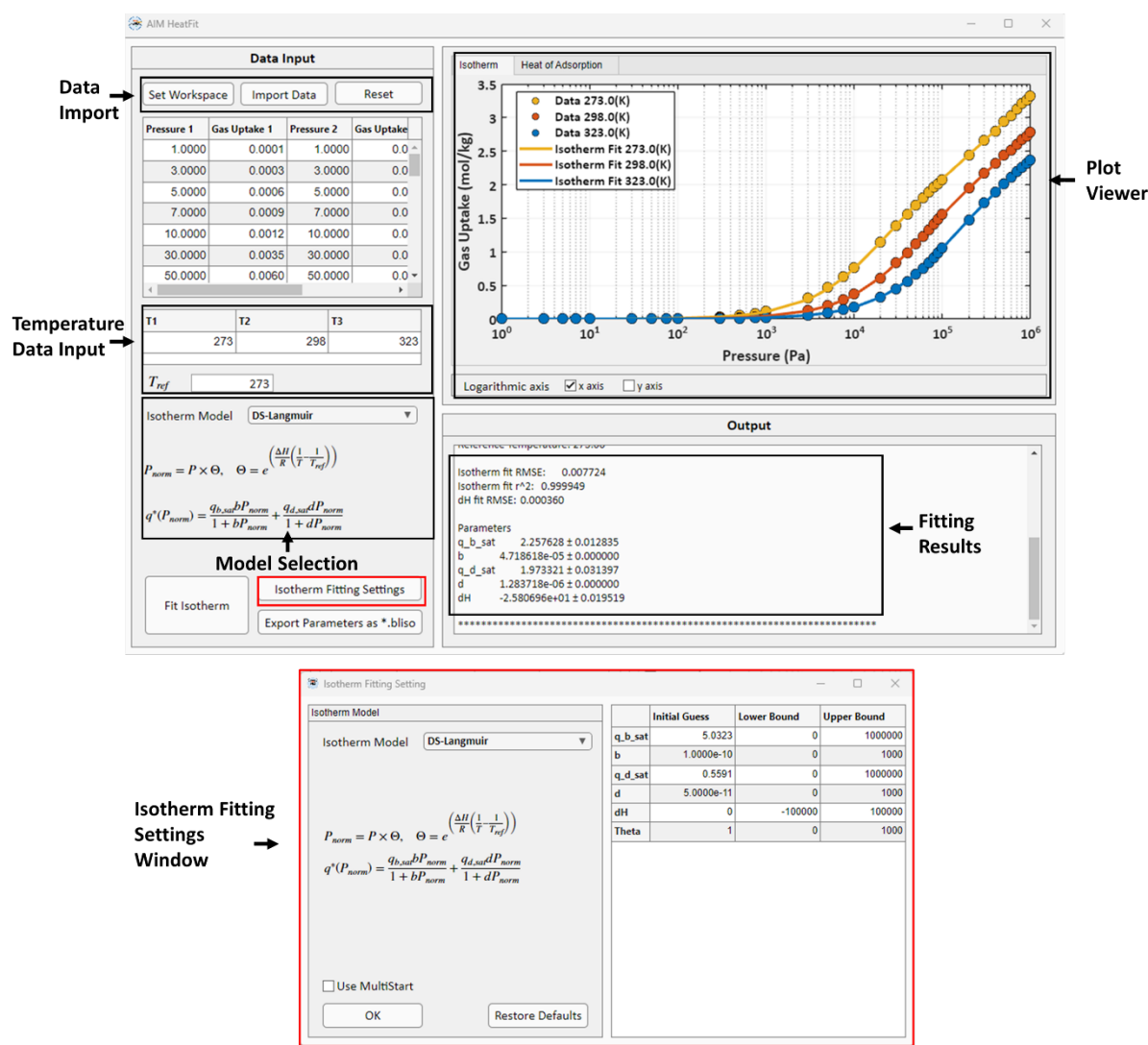


**Fig. 5.** HeatFit GUI with main isotherm fitting interface and Isotherm Fitting Settings dialogue box. **Data Input:** access to loading isotherm data, temperature values corresponding to isotherm data, reference temperature used for fitting, and isotherm model selection for fitting. **Plot Viewer:** displays the fitted isotherm model curve and isotherm data. **Output:** numerical output of fitted parameters and fitting statistics. **Isotherm Fitting Settings:** access to the initialization of the fitting procedure with user-defined initial guesses, upper and lower bounds for isotherm model parameters



#### 4.1. Clausius-Clapeyron equation

The Clausius-Clapeyron is a thermodynamic relationship which expresses the relationship between pressure and temperature for phase change processes. Since adsorption can be considered as a thermodynamic process involving a phase change, the impact of temperature on the adsorption pressure can be calculated by Clausius-Clapeyron equation. The Clausius-Clapeyron equation is given as,

$$\left. \frac{\partial(\ln P)}{\partial T} \right|_q = \frac{-\Delta H_{ads}}{RT^2} \quad (24)$$

where  $\Delta H_{ads}$  and  $R$  are the isosteric enthalpy of adsorption and general gas constant, respectively. For Clausius-Clapeyron implementation in HeatFit, we assumed that the  $\Delta H_{ads}$  is constant for different temperatures and pressure, yielding the following form of Clausius-Clapeyron equation,

$$\ln\left(\frac{P_{ref}}{P}\right) = \frac{-\Delta H_{ads}}{R} \left(\frac{1}{T} - \frac{1}{T_{ref}}\right) \quad (25)$$

where  $P_{ref}, T_{ref}$ , and  $P, T$  are the adsorption pressures and temperatures for the reference state, and given state, respectively. Both the reference state and the given state correspond to a constant adsorption loading  $q$ ,

$$q = f(T, P) = f(T_{ref}, P_{ref}) \quad (26)$$

where  $f(P, T)$  is any isotherm model. Assuming  $f_{ref}$  as the isotherm model fitted at  $T_{ref}$ , which is only the function of  $P$ , we have

$$q = f(T, P) = f_{ref}(P_{ref}) \quad (27)$$

Substituting  $P_{ref}$  value using equation (25),

$$q = f(T, P) = f_{ref} \left( P \times \exp \left( \frac{-\Delta H_{ads}}{R} \left( \frac{1}{T} - \frac{1}{T_{ref}} \right) \right) \right) \quad (28)$$

The utility of equation (28) is that it allows us to predict the loading at different temperatures and pressures using the isotherm model fitted at reference conditions. Additionally, if we have pressure-loading data at different temperatures, and an isotherm model fitted at the reference conditions we can also fit for  $\Delta H_{ads}$ .

#### 4.2. Virial equation

The Virial equation is given as [53],

$$\ln P = \ln q^* + \frac{1}{T} \sum_{i=0}^m a_i (q^*)^i + \sum_{j=0}^n b_j (q^*)^j \quad (29)$$

where  $a_i$ , and  $b_i$  are the fitting parameters also known as Virial coefficients.  $m$  and  $n$  refers to the number of Virial coefficients  $a_i$  and  $b_i$ , respectively. In contrast with the isotherm models discussed earlier, the Virial equation expresses the pressure as a function of adsorption loading. The Virial equation expresses the isosteric heat of adsorption with the loading given as:

$$Q_{st}(q^*) = -R \sum_{i=0}^m a_i (q^*)^i \quad (30)$$

where  $Q_{st}$  is the isosteric heat of adsorption,  $R$  is the general gas constant. The isosteric heat of adsorption for the infinite dilution (i.e. for very low adsorption loading) is expressed as,

$$Q_{st}^0(q^*) = -R a_0 \quad (31)$$

where  $Q_{st}^0$  is the isosteric heat of adsorption at infinite dilution, and  $a_0$  is the first Virial coefficient. The relationship between isosteric heat of adsorption and isosteric enthalpy of adsorption is given as:

$$Q_{st} = -\Delta H_{ads} \quad (32)$$

## 5. MixPred – Mixture adsorption loadings

Adsorption isotherm of mixture depends on the pressure, temperature, and the mixture composition. MixPred module estimates the mixture adsorption loading for the given pressure and composition. **Figure 6** shows the GUI window of MixPred. The isotherm models fitted using IsoFit can be directly loaded in the module. Then, the user can specify the desired pressure range and mixture composition to calculate the mixture loading. The mixture loadings are estimated based on the pure component isotherm models, mixture adsorption model, and the specified mixture composition for the pressure range. The calculated mixture loadings and adsorbed mole fraction are plotted in the Plot viewer and are also reported in the Output panel. The user can also export the calculated mixture loadings in several available file formats. Below we describe the two mixture adsorption isotherm models available in MixPred.

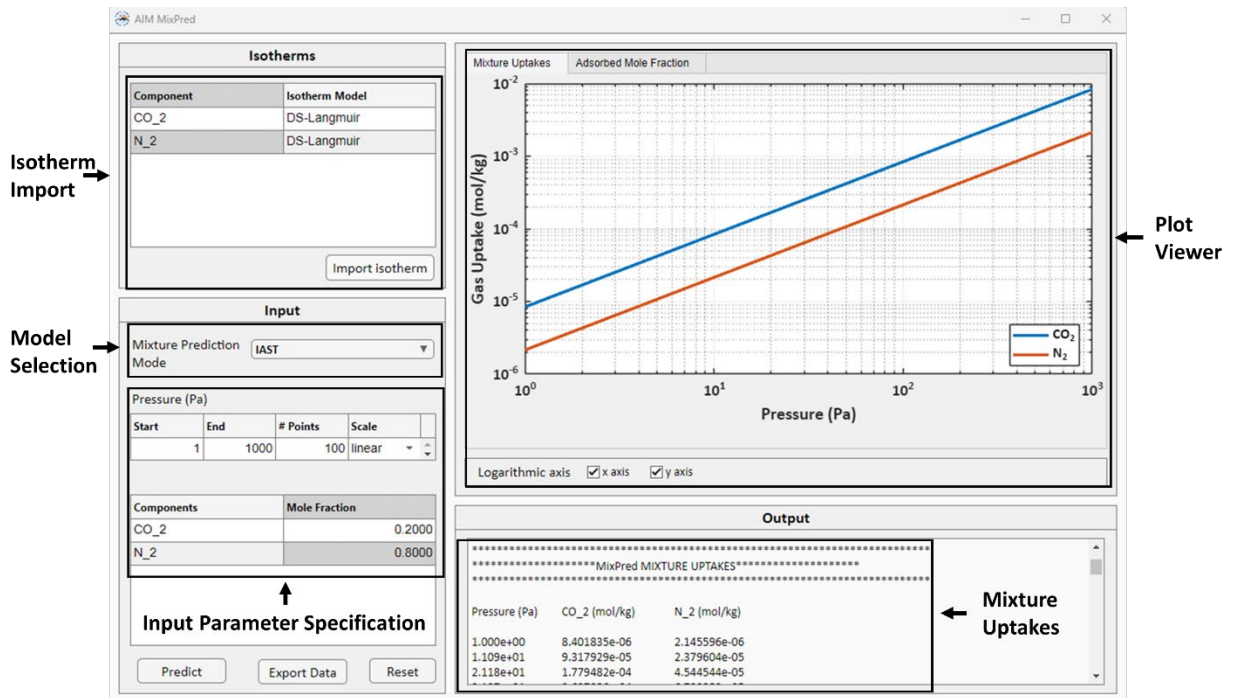


**Fig. 6.** MixPred GUI with main interface. **Isotherms:** access to load isotherm models fitted using IsoFit and HeatFit for different components. **Input:** specify mixture adsorption mode (extended model or IAST), probe pressure points for mixture adsorption loadings, and the mixture

composition. **Plot Viewer:** displays the calculated mixture loadings and adsorbed mole fractions.

**Output:** outputs the calculated mixture loadings

### 5.1. Extended Dual-site Langmuir model (EDSL)

The extended Langmuir model [54,55] is a generalization of the Langmuir model for multi-component adsorption. The model is expressed as

$$q_i^* = \frac{q_{sat,1,i} b_{1,i} P_i}{1 + \sum_1^N b_{1,j} P_j} + \frac{q_{sat,2,i} b_{2,i} P_i}{1 + \sum_1^N b_{2,j} P_j} \quad (33)$$

where  $N$  is the number of components involved;  $q_{sat,1,i}$ ,  $q_{sat,2,i}$ ,  $b_{1,i}$ ,  $b_{2,i}$ , and  $P_i$  are the Langmuir isotherm parameters and partial pressure of component  $i$  respectively. The Langmuir isotherm parameters for individual components can be obtained by fitting Langmuir isotherm model to the isotherm data for the given component. The Extended Langmuir model is thermodynamically consistent only when the saturation capacities  $q_{sat,1}$  and  $q_{sat,2}$  for each component are equal [56], as follows:

$$q_{sat,b1} = q_{sat,b2} = q_{sat,b3} = \cdots q_{sat,bN} \quad (34)$$

$$q_{sat,d1} = q_{sat,d2} = q_{sat,d3} = \cdots q_{sat,dN} \quad (35)$$

### 5.2. Ideal Adsorption Solution Theory (IAST)

IAST is a thermodynamic framework proposed by Mayers and Prausnitz [18] to calculate the mixture isotherms from single-component isotherms. The IAST is based on three fundamental assumptions:

- The surface area of the adsorbent is equally accessible to all adsorbates.
- The adsorbed phase is an ideal solution.
- The adsorbent is homogeneous.

The solution of the IAST involves solving non-linear equations consisting of a reduced grand potential. For the component  $i$ , the reduced grand potential  $\psi_i^*$  is given by [57]

$$\psi_i^* = \int_0^{P_i^*} \frac{q_i^*(P)}{P} dP \quad (36)$$

where  $P_i^*$  is the fictitious pressure, and  $q_i^*$  is the equilibrium loading of component  $i$ . The fictitious pressure,  $P_i^*$  is the pressure for component  $i$  at which it exerts the same reduced grand potential as the other components and is related to the partial pressure of component  $i$ , which is given as:

$$P_i = x_i P_i^* \quad \text{for } i = 1, 2, 3, \dots, N. \quad (37)$$

where  $N$  is the number of adsorbing components;  $P_i$  and  $x_i$  are the partial pressure and adsorbed mole fraction of component  $i$ , respectively.

IAST states that thermodynamic equilibrium is achieved when the reduced grand potential of every component becomes equal.

$$\psi_1^* = \psi_2^* = \psi_3^* = \psi_4^* = \dots \psi_N^* \quad (38)$$

In addition, the sum of the adsorbed mole fraction must be equal to 1:

$$\sum_i x_i = 1 \quad (39)$$

Together, equations (36), (37), (38), and (39) form a set of  $2N$  equations that can be solved for  $2N$  unknowns:  $P_i^*$  and  $x_i$ . The equations in the IAST framework are highly non-linear and often extremely sensitive to the initial conditions [58]. Moreover, the solution is often computationally expensive and time-consuming, especially in breakthrough simulations where IAST equations are solved many times because of the dynamic conditions. It is recommended for the user to use EDSL provided that the user is able to obtain sufficiently good fit of their isotherm data ( $r^2 > 0.99$ ) before proceeding to breakthrough simulation since the results may be sensitive to the fitting results.

## 6. BreakLab - Breakthrough simulation

BreakLab is a GUI module to simulate isothermal/non-isothermal multicomponent breakthrough curves for fixed-bed systems up to 5 components. **Figure 7** shows the BreakLab GUI. BreakLab provides seamless integration of different modules as the isotherm models fitted using IsoFit and HeatFit can be directly loaded into the BreakLab. The breakthrough simulation is run for the given set of isotherm model, and parameters, and the resulting breakthrough curves are displayed. The user can interact with the simulation results using the post-processing features available in BreakLab and can also save the resulting breakthrough data in several file formats.

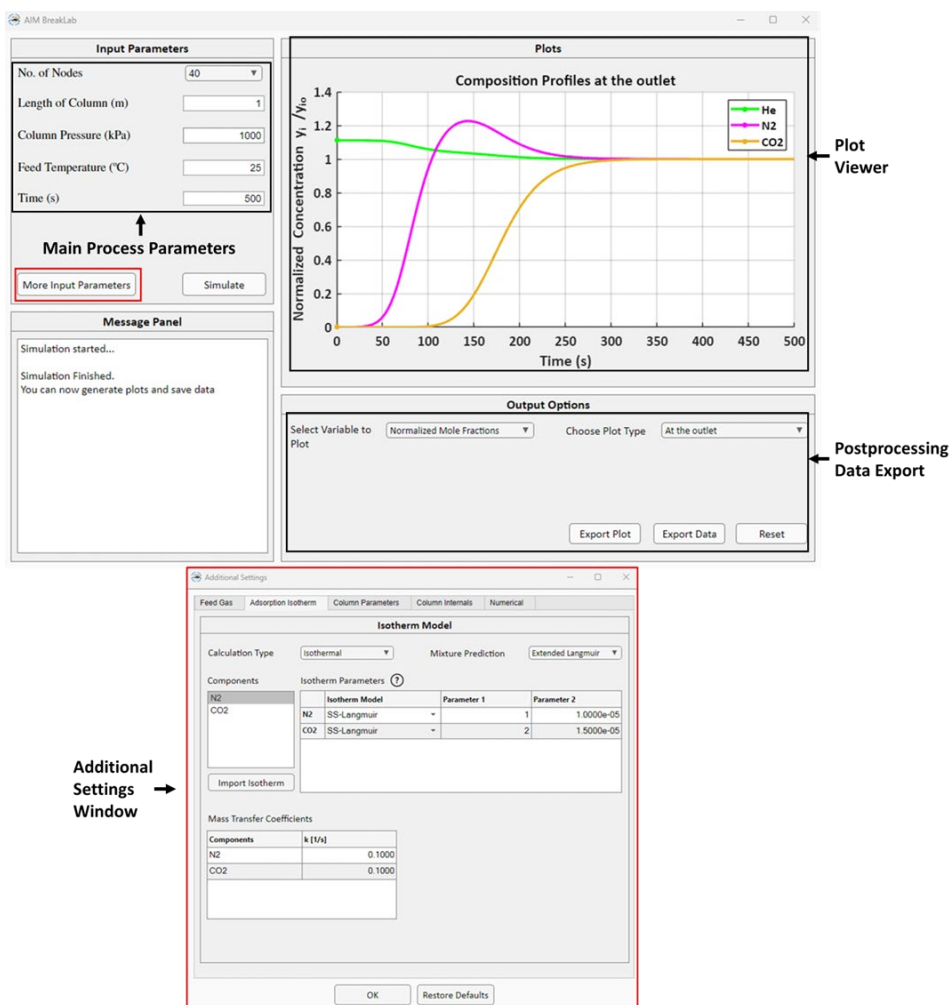


**Fig. 7.** BreakLab (GUI) showing the main breakthrough simulation interface and Additional Settings Window. **Input Parameters:** access to some key process parameters for quick simulation. **Message Panel:** reports simulation messages and any error encountered during the simulation. **Plots:** displays the breakthrough simulation results. **Output Options:** post-processing and data

export options for breakthrough results. **Additional Settings Window:** access to the complete set of required simulation parameters can be opened by clicking “More Input Parameter” button

### 6.1. Model development

The mathematical model describing non-isothermal, non-adiabatic, and non-isobaric fixed bed adsorption phenomena comprises of material, momentum, and energy balances. The underlying assumptions to simplify the mathematical model are as follows:

- The flow is axially dispersed and characterized by an axial dispersion coefficient.
- The gas phase is ideal.
- Pressure-drop across the column is given by the Ergun equation.
- The steady-state momentum balance is applicable.
- The adsorbent bed is uniform; the bed density, void fraction, and particle size are constant throughout the column.
- Thermal equilibrium exists between the solid and gas phase; gas and solid phase temperature is the same.
- The heat transfer coefficient governing the heat transfer between the bed and wall of the column is constant.
- The wall temperature remains constant.
- The mass transfer resistance between the solid and gas phases is governed by the Linear Driving Force (LDF) model.
- The gradients in the radial direction are negligible.

The material, energy, and momentum balances are developed based on the conservation of mass, energy, and momentum in the fixed bed, respectively. These balance equations consist of the mass conservation of species  $i$ , overall mass balance, conservation of the total momentum and the total energy of the system. The balance equations are then simplified based on the assumptions listed above. The mass balance based on the concentration of species  $i$  in the gas phase is given as follows:

$$\varepsilon_t \frac{\partial C_i}{\partial t} = \varepsilon_b \frac{\partial}{\partial z} \left( D_{ax} \frac{\partial C_i}{\partial z} \right) - \varepsilon_b \frac{\partial}{\partial z} (v C_i) - \rho_{b,ads} \frac{\partial q_i}{\partial t} \quad (40)$$

where  $C_i$  is the concentration of species  $i$ ;  $\varepsilon_t$ ,  $\varepsilon_b$ ,  $D_{ax}$ , and  $v$  are the total porosity, bed porosity, axial dispersion coefficient, and interstitial velocity, respectively;  $\rho_{b,ads}$  is the bulk density of adsorbent, and  $q_i$  is the adsorbed molar loading of species  $i$ . The left term in equation (40) represents the accumulation of species  $i$  in the gas phase, while the first, second, and third terms on the right side represent the axial diffusion, convection, and adsorption phenomena, respectively.

BreakLab estimates the axial dispersion coefficient  $D_{ax}$  using the following correlation [1]:

$$D_{ax} = 0.7D_m + v_0r_p \quad (41)$$

where  $D_m$ ,  $v_0$ , and  $r_p$  are the molecular diffusivity of the feed, superficial velocity of the feed, and particle radius, respectively.

The total porosity  $\varepsilon_t$  is calculated as:

$$\varepsilon_t = \varepsilon_b + (1 - \varepsilon_b)\varepsilon_p \quad (42)$$

where  $\varepsilon_p$  is the particle porosity. **Figure 8** illustrates the relationship between different types of porosities. BreakLab uses user-defined bulk and particle porosities.

Based on the ideal gas assumption and Dalton's law of partial pressures, the gas phase concentrations  $C_i$  is related to partial pressure,  $P_i$  as:

$$C_i = \frac{P_i}{RT} = \frac{y_i P}{RT} \quad (43)$$

where  $P$  and  $T$  are the total pressure and temperature of the gas phase, respectively, and  $R$  is the general gas constant. The material balance can be expressed as mole fractions using equation (43).

$$\varepsilon_t \left( \frac{\partial y_i}{\partial t} + \frac{y_i}{P} \frac{\partial P}{\partial t} - \frac{y_i}{T} \frac{\partial T}{\partial t} \right) = D_{ax} \frac{\varepsilon_b T}{P} \frac{\partial}{\partial z} \left( \frac{P}{T} \frac{\partial y_i}{\partial z} \right) - \frac{\varepsilon_b T}{P} \frac{\partial}{\partial z} \left( \frac{y_i v P}{T} \right) - \frac{\rho_{b,ads} RT}{P} \frac{\partial q_i}{\partial t} \quad (44)$$



To close the material balance, an overall material balance equation can be obtained by summing equation (44) over all the components  $i \in N$ , yielding an explicit equation in terms of the total pressure of the system.

$$\frac{\partial P}{\partial t} = \frac{P}{T} \frac{\partial T}{\partial t} - \frac{\varepsilon_b T}{\varepsilon_t} \frac{\partial}{\partial z} \left( \frac{vP}{T} \right) - \frac{\rho_{b,ads} RT}{\varepsilon_t} \sum_{i \in I} \frac{\partial q_i}{\partial t} \quad (45)$$

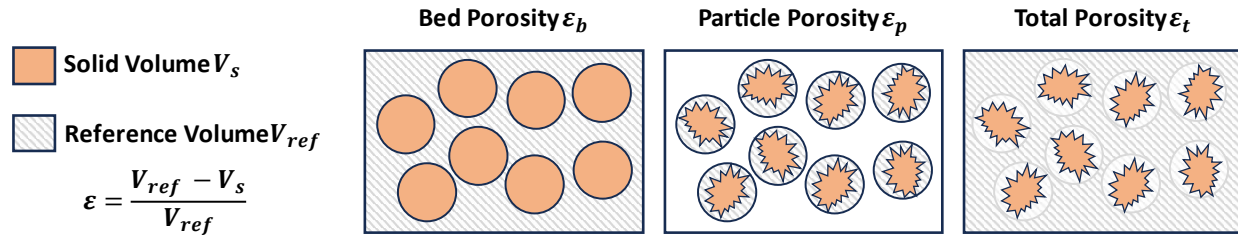


**Fig. 8.** Schematic showing the choice of reference and solid volumes to calculate different types of porosities. Bulk porosity  $\varepsilon_b$  accounts for the free space outside the particles. Particle porosity  $\varepsilon_p$  represents the free space within the particle. The total porosity  $\varepsilon_t$  considers the free volume both outside and inside the particle

For non-isothermal breakthrough simulations, the energy balance is required to calculate temperature changes in the column to account for the heat generated from adsorption. Since the model assumes thermal equilibrium between the gas and solid phase, only gas phase energy balance is required. The energy balance for the gas phase is constructed as:

$$\begin{aligned} & \left( \rho_{b,ads} C_{p,ads} + \rho_{b,ads} C_{p,a} \sum_{i \in I} q_i \right) \frac{\partial T}{\partial t} \\ &= K_z \frac{\partial^2 T}{\partial z^2} - \frac{C_{p,gas} \varepsilon_b}{R} \frac{\partial}{\partial z} (vP) + \rho_{b,ads} \left( \sum_{i \in I} \left( -\Delta H_{ads,i} \frac{\partial q_i}{\partial t} \right) - C_{p,a} T \sum_{i \in I} \frac{\partial q_i}{\partial t} \right) \\ & - \frac{2h_{in}}{r_{in}} (T - T_{wall}) - \frac{C_{p,gas} \varepsilon_t}{R} \frac{\partial P}{\partial t} \end{aligned} \quad (46)$$

where  $K_z$  is the thermal conductivity of gas;  $C_{p,ads}$ ,  $C_{p,a}$ , and  $C_{p,gas}$  are the specific heat capacities of the adsorbent, adsorbed phase, and gas phase, respectively;  $\Delta H_{ads,i}$  is the isosteric heat of adsorption of component  $i$ ;  $h_{in}$ ,  $r_{in}$ , and  $T_{wall}$  are the inside heat transfer coefficient, the radius of

the breakthrough column, and the column wall temperature, respectively. The terms on the right side of the above equation account for the conduction, convection, heat effects due to adsorption, and heat transfer to/from the wall. The last term accounts for the temperature changes due to moles of gas itself. We have assumed that  $C_{p,a}$  is equal to  $C_{p,gas}$  in BreakLab.

With the above energy balance, user can simulate both scenarios; (a) simulation with constant column wall temperature, and (b) adiabatic column by making  $h_{in}$ , the heat transfer coefficient equals to zero.

Ergun equation is used for packed beds to describe the axial pressure drop.

$$-\frac{\partial P}{\partial z} = \left( \frac{150\mu}{4r_p^2} \right) \left( \frac{1 - \varepsilon_b}{\varepsilon_b} \right)^2 v + \left( \frac{1.75\rho_{gas}}{2r_p} \left( \frac{1 - \varepsilon_b}{\varepsilon_b} \right) \right) v^2 \quad (47)$$

where  $\mu$ ,  $r_p$ , and  $\rho_{gas}$  are the viscosity of the gas phase, particle radius, and mass density of the gas, respectively. The mass transfer between the adsorbent and gas phase is given by the linear driving force (LDF) model.

$$\frac{\partial q_i}{\partial t} = k_i(q_i^* - q_i) \quad (48)$$

where  $k_i$  is the mass transfer coefficient of adsorbing species  $i$ , and  $q_i^*$  is the mixture equilibrium molar loading calculated by the user-defined single component isotherm model and parameters. For calculating the mixture equilibrium molar loading, the user can choose between extended Langmuir and IAST. Users can import single component isotherm model parameters obtained from IsoFit or HeatFit or directly choose isotherm model and specify the required parameters for the given component within the BreakLab module. BreakLab uses the user-defined mass transfer coefficients.

## 6.2. Boundary conditions

Two different types of boundary conditions are used for the adsorption processes. In BreakLab, the Danckwerts boundary conditions [59,60] are used for the dispersed plug flow system. **Table 3** lists the boundary conditions implemented for the breakthrough simulation.

Equations (42-48) along with the boundary conditions constitute the complete mathematical model of BreakLab. **Table 4** summarizes all the physical input parameters required in BreakLab for running breakthrough simulation.

**Table 3.** Boundary conditions implemented in BreakLab

		Inlet boundary	Outlet boundary
Mole fraction	$y_i$	$D_{ax} \frac{\partial y_i}{\partial z} \Big _{z=0} = -v _{z=0}(y_{i,0} - y_i _{z=0})$	$\frac{\partial y_i}{\partial z} \Big _{z=L} = 0$
Temperature	$T$	$K_Z \frac{\partial T}{\partial z} \Big _{z=0} = -\varepsilon_b v _{z=0} \rho_{gas} C_{p,gas} (T_0 - T _{z=0})$	$\frac{\partial T}{\partial z} \Big _{z=L} = 0$
Velocity	$v$	$v _{z=0} = v_0$	—
Pressure	$P$	$P _{z=0} = f(v)$	$P _{z=L} = P_0$

**Table 4.** List of physical parameters required for breakthrough simulation in BreakLab

Parameters	Description	Units
<b>Feed Gas</b>		
$T_0$	Feed gas temperature	°C
$v_0$	Superficial velocity of feed gas	ms <sup>-1</sup> OR std cm <sup>3</sup> min <sup>-1</sup>
$y_{i,0}$	Feed gas mole fraction of component $i$	—
$MW_i$	Molecular weight of component $i$	kg mol <sup>-1</sup>
$D_m$	Molecular diffusivity of gas	m <sup>2</sup> s <sup>-1</sup>
$K_z$	Thermal conductivity of gas	W m <sup>-1</sup> °C <sup>-1</sup>
$C_{p,gas}$	Specific heat capacity of gas	J mol <sup>-1</sup> °C <sup>-1</sup>
$\mu$	Viscosity of gas	Pa. s
<b>Fixed Bed Column</b>		
$P_0$	Pressure of fixed bed column	kPa
$L$	Total length of fixed bed column	m
$D_{col}$	Diameter of fixed bed column	m
$h_{in}$	Fixed bed column inside heat transfer coefficient	W m <sup>-2</sup> °C <sup>-1</sup>
$T_{wall}$	Temperature of fixed bed column wall	°C
<b>Fixed Bed Column Internal</b>		
$\rho_{b,ads}$	Adsorbent bulk density	kgm <sup>-3</sup>
$D_p$	Diameter of adsorbent particles	m
$\varepsilon_b$	Bulk porosity	—
$\varepsilon_p$	Particle porosity	—
$C_{p,ads}$	Specific heat capacity of adsorbent bed	J kg <sup>-1</sup> °C <sup>-1</sup>
<b>Adsorption Isotherm</b>		
Isotherm Parameters	Isotherm parameters for the chosen isotherm model.	Various units
$\Delta H_{ads,i}$	Isosteric heat of adsorption for component $i$	kJ mol <sup>-1</sup>
$T_{ref}$	Reference temperature for isotherm fitting	K
$k_i$	Mass transfer coefficient of component $i$	s <sup>-1</sup>

## 7. Numerical methods

In this section, we discuss the underlying numerical procedures for isotherm fitting and breakthrough simulation in IsoFit, HeatFit and BreakLab modules.

### 7.1. Isotherm fitting in IsoFit

In IsoFit, the isotherm fitting is done using non-linear regression by minimizing the sum of squared error (*SSE*) function:

$$SSE = \min_{a_k} \sum_i^N (q_{i,exp}^* - f(P_i; \{a_k\}_1^M))^2 \quad (49)$$

where  $N$  and  $q_{i,exp}^*$  represents the total number of data points and the experimental gas uptake for the given data point  $i$ , respectively.  $f(P_i; \{a_k\}_1^M)$  is the isotherm model where,  $P_i$  is the pressure value for the given data point  $i$ ,  $a_k$  is the set of parameters and  $M$  is the total number of parameters for the given isotherm model.

In IsoFit, regression is performed using the MATLAB's built-in non-linear least square solver *lsqnonlin* [61]. The user can control the regression process by specifying custom initial guesses, as well as lower and upper bounds. Additionally, IsoFit offers a multistart option, which generates 1000 random initial guess within the specified bounds. The fitting process is then performed sequentially for each initial guess and the best fitting result is selected. The multistart approach is useful for fitting problems with multiple parameter solutions. In such cases, fitting using multistart option can identify the global minimum corresponding to the best parameter estimates. The multistart option is available for all isotherm models except 'Auto' mode. In 'Auto' mode, IsoFit performs isotherm fitting using all the available isotherm models and then selects the best model. Using multistart option for 'Auto' mode can be computationally expensive leading to excessive running times.

Root mean square error (RMSE) is used in the program to evaluate the goodness of fit.

$$RMSE = \sqrt{\frac{SSE}{N - M}} \quad (50)$$

where  $N$  and  $M$  are the total number of data points and the number of parameters in the isotherm model, respectively. If the user chooses the ‘Auto’ mode, IsoFit reports the best isotherm model with the lowest RMSE values. If two or more models have same value of  $SSE$ , then IsoFit will choose the model with a smaller number of parameters because of lower value of RMSE .

IsoFit also reports coefficient of determination,  $r^2$ , value defined as:

$$r^2 = 1 - \frac{SSE}{\sum (q_{i,exp}^* - \overline{q_{i,exp}^*})^2} \quad (51)$$

where  $\overline{q_{i,exp}^*}$  is the mean value of experimental gas uptakes.

## 7.2. Isotherm fitting in HeatFit

In HeatFit, the isotherm fitting and prediction of the isosteric heat of adsorption can be carried out using either the Clausius-Clapeyron or Virial equations. Fitting method varies based on the chosen model.

### 7.2.1. Clausius-Clapeyron

HeatFit uses the methodology devised by Ga *et al.* [27]. The method involves three steps which are as follows,

- Step 1: Isotherm fitting at reference temperature
- Step 2: Fitting for  $\Theta$  parameter
- Step 3: Fitting for isosteric heat of adsorption  $\Delta H_{ads}$

In all three steps, regression is performed using MATLAB built-in *lsqnonlin* solver [61]. The user can control the regression process using different sets of values for initial guesses, lower and upper bounds.

#### Step 1: Isotherm fitting at reference temperature

Like IsoFit, the isotherm fitting at reference temperature is done using non-linear regression. The objective is to minimize the  $SSE$  function given as,

$$SSE = \min_{a_k} \sum_i^N (q_{i,exp}^* - f(P_i; \{a_k\}_1^M))^2 \quad (52)$$

where  $N$  and  $q_{i,exp}^*$  represents the total number of data points and the experimental gas uptake for the given data point  $i$  at reference temperature, respectively.  $f(P_{i,ref}; \{a_k\}_1^M)$  is the isotherm model where,  $P_i$  is the pressure value for the given data point  $i$  at reference temperature,  $a_k$  is the set of parameters and  $M$  is the total number of parameters for the given isotherm model. Similar to IsoFit, HeatFit also supports user-defined initial guesses, lower and upper bounds, and multistart option for controlling the regression process.

The program uses the RMSE to evaluate the goodness of fit. RMSE is calculated as:

$$RMSE = \sqrt{\frac{SSE}{N - M}} \quad (53)$$

where  $N$  and  $M$  are the total number data points and the number of parameters in the isotherm model, respectively. If the user chooses the ‘Auto’ mode, the program will choose the best isotherm model with lowest value of RMSE for prediction of  $\Delta H_{ads}$ . Additionally, if two or more models have same value of  $SSE$ , then the program will choose the model with a smaller number of parameters. In addition to RMSE, HeatFit reports  $r^2$  value which is defined as:

$$r^2 = 1 - \frac{SSE}{\sum (q_{i,exp}^* - \overline{q_{i,exp}^*})^2} \quad (54)$$

where  $\overline{q_{i,exp}^*}$  is the mean value of experimental gas uptakes at reference temperature.

## Step 2: Fitting for $\Theta$ parameter

Second step involves using the isotherm model and the parameters obtained from fitting at reference temperature to get a set of parameters  $\Theta$ , which is defined as,

$$\Theta = \{\theta_j\}_{j=1}^Z \quad (55)$$

where  $Z$  is the total number of temperature values used in the fitting process. Every  $\theta_j$  value in the  $\Theta$  vector corresponds to temperature value  $T_j$ . Then the program uses non-linear regression to fit for each  $\theta_j$  value with the objective function defined as follows,

$$SSE = \min_{\theta_j} \left( q_{j,exp}^* - g(P; \theta_j) \right)^2 \quad (56)$$

where  $q_{j,exp}^*$  is the experimental gas uptake at temperature  $T_j$  while  $g(P; \theta_j)$  can be expressed as,

$$g(P; \theta_j) = f_{ref} \left( P \times \theta_j; \{a_{k,ref}\}_{k=1}^M \right) \quad (57)$$

where  $f_{ref}$  and  $a_{k,ref}$  represents the isotherm function and isotherm function parameters obtained in step 1 using reference conditions, respectively.

### Step 3: Fitting for $\Delta H_{ads}$

Next, the correlation between  $\theta_j$  and  $T_j$  is used to fit for  $\Delta H_{ads}$ . The correlation is given by the Clausius-Clapeyron equation as:

$$\theta_{j,pred} = \exp \left( \frac{-\Delta H_{ads}}{R} \left( \frac{1}{T_j} - \frac{1}{T_{ref}} \right) \right) \quad (58)$$

The program uses non-linear regression to fit for  $\Delta H_{ads}$  value while minimizing the objective function defined as:

$$SSE = \min_{\Delta H_{ads}} \sum_{j=1}^Z (\theta_j - \theta_{j,pred}) \quad (59)$$



The program also reports the RMSE value for  $\Delta H_{ads}$  fitting. The RMSE value is evaluated as:

$$RMSE = \sqrt{\frac{SSE}{Z}} \quad (60)$$

### 7.2.2. Virial equation

In the case of using Virial equation, the program performs curve fitting for the entire Virial equation parameters and then the isosteric heat of adsorption is calculated using equation (30) and (31). The fitting of Virial equation is carried out in a similar manner to the isotherm model fitting procedure described in IsoFit section (**section 7.1**). The only exception is the definition of sum of squared error function which in the case of Virial equation is

$$SSE = \min_{a_k} \sum_i^N \left( \ln(P_{i,exp}) - f(q_{i,exp}^*, T_i; \{a_k\}_1^M) \right)^2 \quad (61)$$

Where  $N$  is the total number of data points,  $P_{i,exp}$ ,  $q_{i,exp}^*$ , and  $T_i$  are the experimental pressure value, experimental gas uptake, and temperature values for the given data point  $i$ , respectively.  $a_k$  and  $M$  represent the  $k^{th}$  Virial parameter and total number of the Virial parameters, respectively.  $f$  is the Virial equation given in equation (29). This form of  $SSE$  is used because the Virial equation expresses the natural logarithm of adsorption pressure as a function of adsorption uptake and temperature.

### 7.3. Numerical solution in BreakLab

In BreakLab, the approach developed by Leperi *et al.* [62] and later extended by Yancy-Caballero *et al.* [63] is used to solve the systems of coupled model PDEs. This work extended the number of components from two to five, implemented different isotherm models, and integrated the solver for the IAST equations.

The model equations are nondimensionalized to resolve the steep gradients in the adsorption processes and for faster convergence. The non-dimensional variables used for nondimensionalization are as follows:

$$\begin{aligned} \bar{P} &= \frac{P}{P_0}, & \bar{T} &= \frac{T}{T_0}, & \bar{v} &= \frac{v}{v_0}, \\ x_i &= \frac{q_i}{q_{i0}}, & \xi &= \frac{z}{L}, & \tau &= \frac{tv_0}{L}, & \bar{T}_{wall} &= \frac{T_{wall}}{T_0} \end{aligned} \quad (62)$$

where  $\bar{P}$ ,  $\bar{T}$ , and  $\bar{v}$  are the dimensionless gas phase pressure, temperature, and interstitial velocity respectively;  $x_i$  is dimensionless loading of species  $i$ ;  $\xi$  is the dimensionless length and  $\tau$  is the dimensionless time.

The dimensionless model equations are derived using the scaled variables in equation (56). **Table 5** lists the dimensionless model equation and parameters. Spatial discretization of the model equations is performed using the finite volume method (FVM) [64] and the weighted essentially non-oscillatory (WENO) scheme [65]. Spatial discretization converts the PDEs into a system of coupled ordinary differential equations ODEs. BreakLab uses MATLAB's built-in stiff ODE solver ode15s [66] for solving the system of ODEs.

**Table 5.** Dimensionless model equations and groups used in BreakLab mathematical model

---

**Component mass balance**

$$\frac{\partial y_i}{\partial \tau} = \frac{\varepsilon_b}{\varepsilon_t P e} \frac{\bar{T}}{\bar{P}} \frac{\partial}{\partial \xi} \left( \frac{\bar{P}}{\bar{T}} \frac{\partial y_i}{\partial \xi} \right) - \frac{\varepsilon_b}{\varepsilon_t \bar{P}} \frac{\partial}{\partial \xi} \left( \frac{y_i \bar{v} \bar{P}}{\bar{T}} \right) - \psi_{ads} \frac{\bar{T}}{\bar{P}} \frac{\partial x_i}{\partial \tau} - \frac{y_i}{\bar{P}} \frac{\partial \bar{P}}{\partial \tau} + \frac{y_i}{\bar{T}} \frac{\partial \bar{T}}{\partial \tau}$$

**Overall mass balance**

$$\frac{\partial \bar{P}}{\partial \tau} = \frac{\bar{P}}{\bar{T}} \frac{\partial \bar{T}}{\partial \tau} - \frac{\varepsilon_b \bar{T}}{\varepsilon_t} \frac{\partial}{\partial \xi} \left( \frac{\bar{v} \bar{P}}{\bar{T}} \right) - \bar{T} \psi_{ads} \sum_{i \in I} \frac{\partial x_i}{\partial \tau}$$

**Energy balance**

$$\frac{\partial \bar{T}}{\partial \tau} = \Omega_1 \frac{\partial^2 \bar{T}}{\partial \xi^2} - \Omega_2 \frac{\partial}{\partial \xi} (\bar{v} \bar{P}) + \sum_{i \in I} \left( \sigma_{i,ads} \frac{\partial x_i}{\partial \tau} \right) - \Omega_3 \bar{T} \sum_{i \in I} \frac{\partial x_i}{\partial \tau} - \Omega_4 (\bar{T} - \bar{T}_{wall}) - \Omega_5 \frac{\partial P}{\partial t}$$

**Momentum balance**

$$-\frac{\partial \bar{P}}{\partial \xi} = \left( \frac{150 \mu L v_0}{4 r_p^2 P_0} \right) \left( \frac{1 - \varepsilon_b}{\varepsilon_b} \right)^2 \bar{v} + \left( \frac{1.75 L v_0^2}{2 r_p T_0} \left( \frac{1 - \varepsilon_b}{\varepsilon_b} \right) \left( \sum_i \frac{M W_i y_i \bar{P}}{R \bar{T}} \right) \right) \bar{v} \|\bar{v}\|$$

**Linear driving force model**

$$\frac{\partial x_i}{\partial \tau} = \alpha_i (x_i^* - x_i)$$

**Dimensionless groups**

$$Pe = \frac{L v_0}{D_{ax}}, \quad \psi_{ads} = \frac{R T_0 q_0 \rho_{b,ads}}{P_0 \varepsilon_t}, \quad \sigma_{i,ads} = \frac{\rho_{b,ads} q_0 (-\Delta H_{ads,i})}{T_0 \Psi}, \quad \alpha_i = \frac{k_i L}{v_0}$$

$$\Omega_1 = \frac{K_z}{L v_0 \Psi}, \quad \Omega_2 = \frac{C_{pg} \varepsilon_b P_0}{R T_0 \Psi}, \quad \Omega_3 = \frac{C_{p,a} \rho_{b,ads} q_0}{\Psi}, \quad \Omega_4 = \frac{2 h_{in} L}{r_{in} v_0 \Psi},$$

$$\Omega_5 = \frac{C_{pg} \varepsilon_t P_0}{R T_0 \Psi}, \quad \Psi = \left[ \rho_{b,ads} C_{p,ads} + C_{p,a} \rho_{b,ads} q_0 \sum_i x_i \right]$$


---

## 8. Case studies using AIM modules

This section details case studies for isotherm fitting and breakthrough simulations conducted using AIM. First, the case study for isotherm fitting for single temperature using IsoFit is presented followed by the breakthrough simulations for isothermal cases. Next, we demonstrate the use of HeatFit for multi-temperature isotherm fitting and isosteric heat of adsorption prediction. Finally, the results for a non-isothermal breakthrough simulation are reported to highlight the non-isothermal simulation capabilities of the BreakLab.

### 8.1. Single temperature isotherm fitting using IsoFit

To demonstrate use of IsoFit module, we considered an adsorption isotherm fitting case study for CO<sub>2</sub> in CALF-20 at 298K. The CO<sub>2</sub> adsorption isotherm data at 298K were obtained using the grand canonical Monte Carlo (GCMC) simulations. The details of the GCMC simulation can be found in **Appendix A**. The isotherm data and the fitted model using IsoFit are shown in **Figure 9a**. The isotherm exhibits an inflection point at 10<sup>3</sup> Pa, indicating the presence of two distinct adsorption sites. We considered the dual-site Langmuir (DSL) isotherm model with four parameters ( $q_{sat,1}$ ,  $b_1$ ,  $q_{sat,2}$ , and  $b_2$ ) based on the above observation. **Figure 9a** shows that IsoFit accurately fits the isotherm data. We also compared the IsoFit fitting results with other isotherm fitting codes which are RUPTURA, IAST+, and pyIAST, as shown in **Table 6**. IsoFit, RUPTURA, and pyIAST give good fit with  $r^2 = 0.9990$  and RMSE < 0.0577. Fitting using IAST++ has a slightly higher RMSE value of 0.0626.

For the fitted isotherm models, we consider uncertainty quantification to assess the robustness of fitting parameters given the uncertainty in the isotherm data itself. In our case, the data has been obtained from GCMC simulation. GCMC is a molecular simulation technique in which adsorption uptake is calculated by sampling the probability distribution from the grand canonical ensemble. The stochastic nature of GCMC sampling can give rise to noise in the calculated uptake. The uncertainty quantification has been performed using the Bayesian inference analysis framework described and implemented by Ward *et al.* [67]. The details about the uncertainty quantification can be found in **Appendix B**. **Figure 9b** shows the probability distribution obtained from the Bayesian inference analysis. The parameters  $\mu$  and  $\sigma$  are the mean and standard deviation of the parameter distributions, respectively.  $\mu$  represents the best value of the parameter while  $\sigma$  indicates the uncertainty associated with the model parameters. Comparing **Figure 9b** with **Table**

6, we observe good agreement between the isotherm parameters obtained from IsoFit and Bayesian analysis which further validates the IsoFit results. In all the isotherm parameters distribution, the corresponding  $\sigma$  value is order of magnitude smaller than the  $\mu$  values which shows that the DSL isotherm model and the parameters obtained from IsoFit accurately describe the isotherm data.

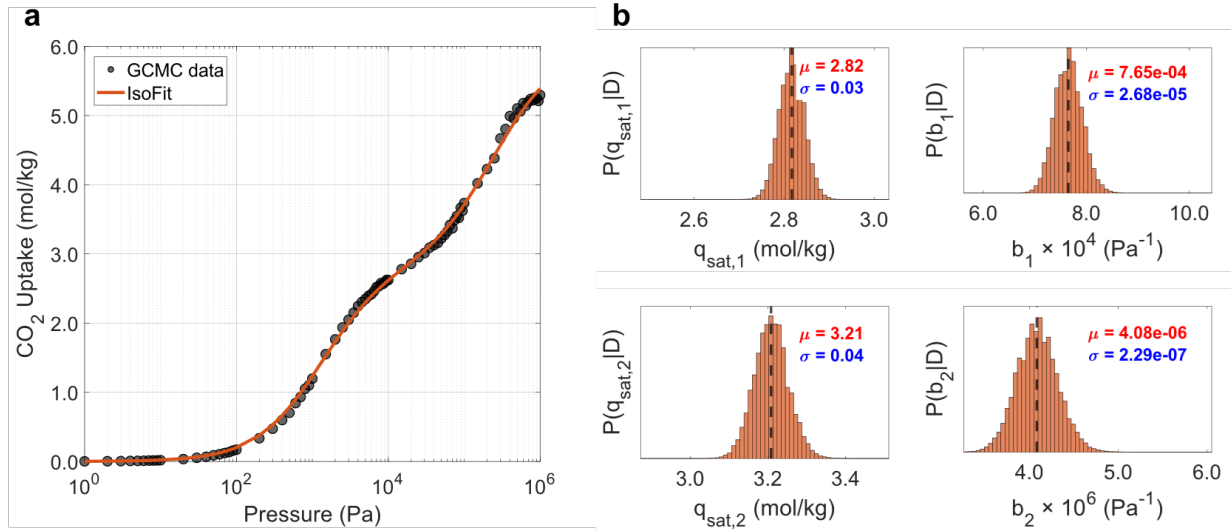


**Fig. 9.** Isotherm fitting results for CO<sub>2</sub> adsorption in CALF-20 at 298K **a.** Dual-site Langmuir (DSL) model fit using IsoFit. Filled circles and solid lines represent the CO<sub>2</sub> uptakes from GCMC simulation and IsoFit model, respectively. **b.** Result of the uncertainty quantification for the fitted DSL model parameters. The dashed line indicates the parameter values as predicted using IsoFit.  $\mu$  and  $\sigma$  are the mean and standard deviation values of the corresponding parameter distributions

**Table 6.** Fitted parameters of dual-site Langmuir model (DSL) for CO<sub>2</sub> adsorption in CALF-20 at 298K using different fitting methods.

<b>Method</b>	<b><math>q_{sat,1}</math> (mol kg<sup>-1</sup>)</b>	<b><math>b_1</math> (Pa<sup>-1</sup>)</b>	<b><math>q_{sat,2}</math> (mol kg<sup>-1</sup>)</b>	<b><math>b_2</math> (Pa<sup>-1</sup>)</b>	<b><math>r^2</math></b>	<b>RMSE</b>
IsoFit	2.82	$7.65 \times 10^{-4}$	3.21	$4.08 \times 10^{-6}$	0.9990	0.0571
RUPTURA	3.21	$4.08 \times 10^{-6}$	2.82	$7.65 \times 10^{-4}$	0.9990	0.0571
IAST ++	2.91	$6.82 \times 10^{-4}$	3.27	$3.33 \times 10^{-6}$	0.9988	0.0626
pyIAST	3.21	$4.00 \times 10^{-6}$	2.82	$7.65 \times 10^{-4}$	0.9990	0.0577

## 8.2. Isothermal breakthrough simulations using BreakLab

Two separation systems have been considered for the isothermal (no energy balance) breakthrough simulations: (1) Xe and Kr separation in SBMOF-1, and (2) CH<sub>4</sub> and CO<sub>2</sub> separation in CALF-20. In both systems, the column packed with the adsorbent is initially filled with He, which is assumed to be a non-adsorbing carrier gas. A gas mixture containing He and (1) Xe/Kr or (2) CO<sub>2</sub>/CH<sub>4</sub> is introduced at the column inlet. The pure component adsorption isotherms at 298K have been obtained using the GCMC simulations and fitted to Langmuir isotherm model using IsoFit module. **Figure 10** shows the GCMC data, and the isotherm fit for the two systems. **Tables 7** and **8** list the isotherm parameters for the two systems, respectively. The parameters for Xe, Kr, and CH<sub>4</sub> correspond to the single-site Langmuir (SSL) model while for CO<sub>2</sub> dual-site Langmuir (DSL) model gives the best fit. **Figure 10** shows that Xe has a higher affinity than Kr for SBMOF-1, while CALF-20 is more selective for CO<sub>2</sub> than CH<sub>4</sub>.

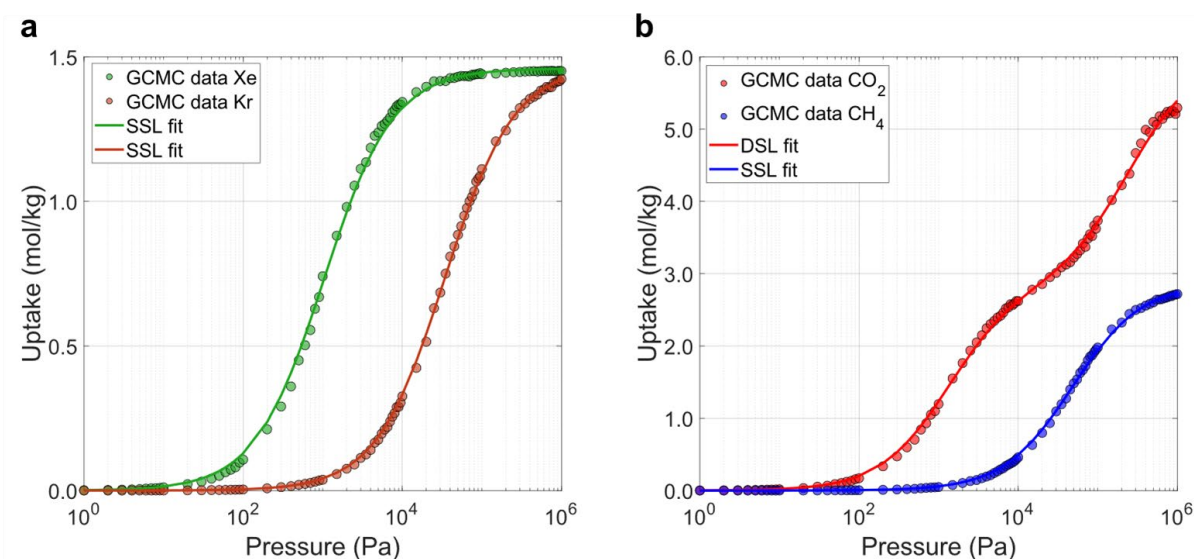


**Fig. 10.** Pure component isotherm fitting results from IsoFit: **a.** Xe/Kr adsorption in SBMOF-1, **b.** CO<sub>2</sub>/CH<sub>4</sub> adsorption in CALF-20, with filled circles representing GCMC simulation data and solid lines showing fitting single-site (SSL) and dual-site (DSL) Langmuir models

**Table 7.** Isotherm parameters for Xe/Kr adsorption in SBMOF-1

Parameters	Xe	Kr	Units
$q_{sat,1}$	1.46	1.47	mol kg <sup>-1</sup>
$b_1$	$9.68 \times 10^{-4}$	$2.92 \times 10^{-5}$	Pa <sup>-1</sup>
$r^2$	0.9992	0.9998	—

**Table 8.** Isotherm parameters for CO<sub>2</sub>/CH<sub>4</sub> adsorption in CALF-20

Parameters	CO <sub>2</sub>	CH <sub>4</sub>	Units
$q_{sat,1}$	2.82	2.87	mol kg <sup>-1</sup>
$b_1$	$7.65 \times 10^{-4}$	$2.08 \times 10^{-5}$	Pa <sup>-1</sup>
$q_{sat,2}$	3.21	—	mol kg <sup>-1</sup>
$b_2$	$4.08 \times 10^{-6}$	—	Pa <sup>-1</sup>
$r^2$	0.9990	0.9994	—

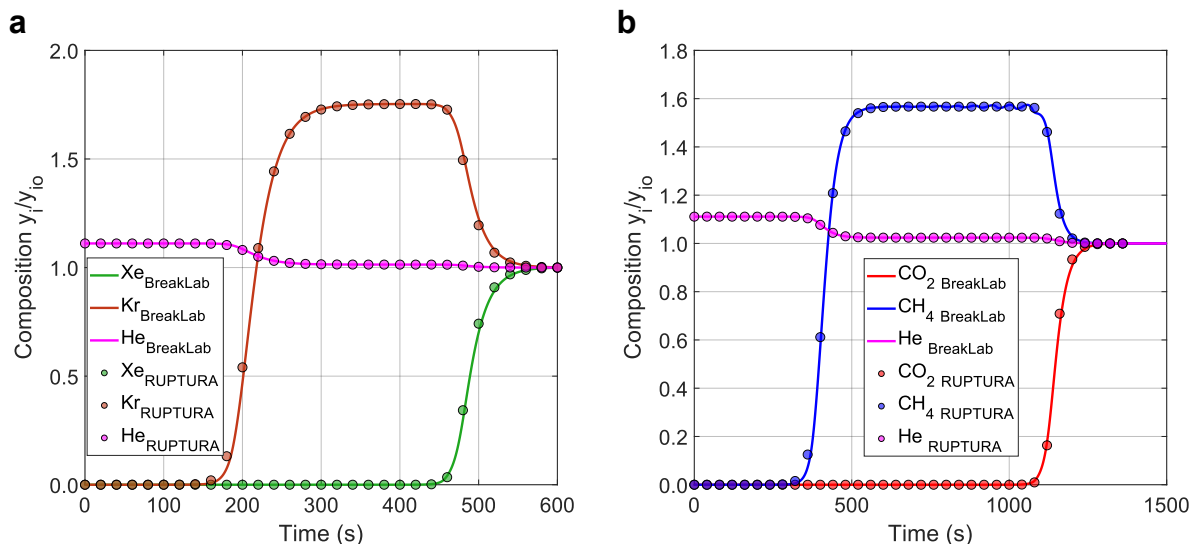
An isothermal breakthrough simulation has been performed for both systems in BreakLab using the fitted isotherm parameters. **Table 9** lists the parameters used in the breakthrough simulation.

**Table 9.** Operating parameters for Xe/Kr and CO<sub>2</sub>/CH<sub>4</sub> breakthrough simulations

Parameters		Value	Units
<i>Feed gas</i>			
Temperature		25	°C
Molecular diffusivity		$1.60 \times 10^{-5}$	m <sup>2</sup> s <sup>-1</sup>
Gas viscosity		$1.72 \times 10^{-5}$	kg m <sup>-1</sup> s <sup>-1</sup>
Feed velocity		0.04	m s <sup>-1</sup>
Mass transfer coefficient		0.10	s <sup>-1</sup>
Composition (mole fraction)	Xe: Kr: He	0.05:0.05:0.90	—
	CO <sub>2</sub> : CH <sub>4</sub> : He	0.05:0.05:0.90	—
<i>Adsorber column</i>			
Pressure		1000	kPa
Length		0.3	m
Diameter		0.0127	m
Particle diameter		$2 \times 10^{-3}$	m
Particle porosity		0.0	—
Bed porosity		0.40	—
Adsorbent bulk density	SBMOF-1	942	kg m <sup>-3</sup>
	CALF-20	959	kg m <sup>-3</sup>

**Figure 11** shows the breakthrough simulation results from both BreakLab and RUPTURA [26]. The IAST model has been used to calculate the mixture adsorption isotherm in both programs. For SBMOF-1 (**Figure 11a**), Kr breakthrough occurs before Xe because of the strong adsorption of Xe compared to Kr. Before Xe breakthrough, the Kr concentration in the outlet gas was higher





than the Kr concentration in the inlet gas. This phenomenon is called roll-up, and the roll-up of the Kr composition occurs because of the lower concentration of strongly adsorbing component Xe in the gas phase and the displacement of already adsorbed Kr back into the gas phase by Xe. Therefore, the concentration of weakly adsorbing components increases in the gas phase and eventually becomes greater than the inlet concentration. Once Xe breakthrough occurs, the concentration of both Xe and Kr becomes equal to the inlet concentration. For CALF-20 (**Figure 11b**), CH<sub>4</sub> breakthrough occurred before CO<sub>2</sub>, showing that CALF-20 has a greater uptake for CO<sub>2</sub> than CH<sub>4</sub>. A similar roll-up behavior is also observed here for CH<sub>4</sub>. **Figure 11** also shows that the results from BreakLab and RUPTURA are in excellent agreement.

**Fig. 11.** Breakthrough curves at the outlet of the adsorber column for: **a.** Xe/Kr in SBMOF-1 and **b.** CO<sub>2</sub>/CH<sub>4</sub> in CALF-20, comparing BreakLab (solid lines) and RUPTURA (filled circles) using IAST

The breakthrough simulation results from BreakLab using IAST and EDSL models are also compared to demonstrate the ability of BreakLab to simulate breakthrough curves using either IAST or EDSL models. **Figure 12** presents the results of such a comparison. The results from the IAST and EDSL models are nearly identical for both adsorption systems.

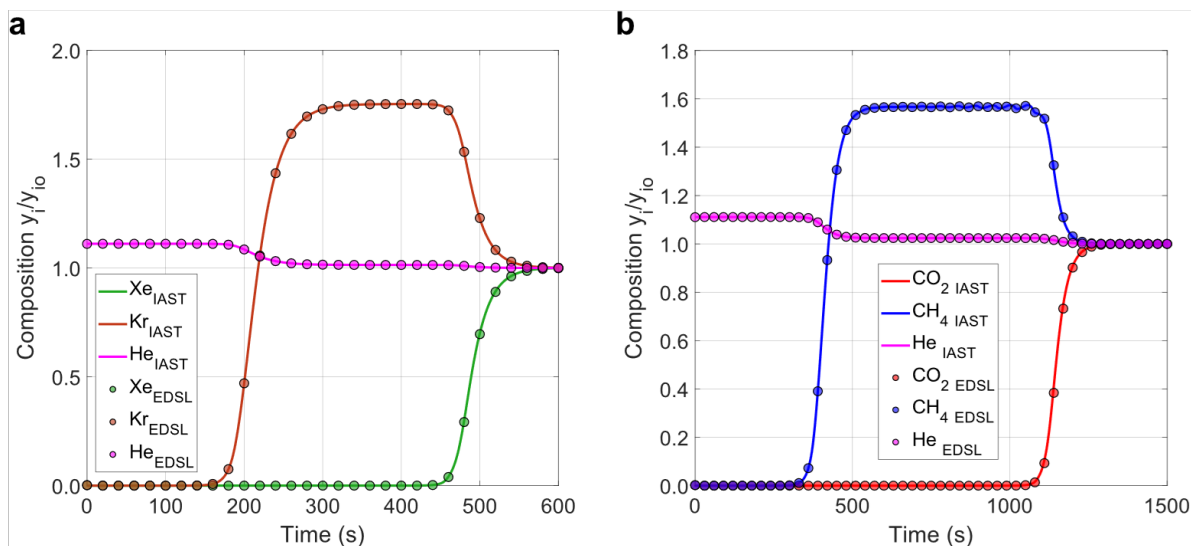


**Fig. 12.** Breakthrough curves obtained from BreakLab at the outlet of the adsorber column using the IAST and EDSL for: **a.** Xe/Kr adsorption in SBMOF-1 and **b.** CO<sub>2</sub>/CH<sub>4</sub> adsorption in CALF-20. Filled circles and solid lines represent the breakthrough results using EDSL and IAST models, respectively

### 8.3. Estimating the Isosteric heat of adsorption using HeatFit

CO<sub>2</sub> adsorption isotherm for CALF-20 were obtained at 273K, 298K, and 323K using GCMC simulation and fitted using Virial equation. Fitting multi-temperature isotherm using Virial equation is often challenging because the same sets of Virial parameters  $a_i$  and  $b_j$  describing isotherm data at all temperatures are sought. Hence, the selection of the number of Virial parameters  $a_i$  and  $b_j$  is critical for ensuring fitting accuracy and reliability. Using a few numbers of parameters can lead to poor fitting while excessive number of parameters can lead to overfitting with unreliable fitting parameters. The common practice is to gradually increase the number of Virial parameters until the RMSE value does not decrease significantly.

To demonstrate the effect of the number of Virial parameters on fitting results, we fitted the Virial equation using HeatFit with: (1) 2  $a_i$  and 1  $b_j$  parameters, (2) 3  $a_i$  and 2  $b_j$  parameters, (3) 5  $a_i$  and 2  $b_j$  parameters, and (4) 7  $a_i$  and 2  $b_j$  parameters. **Figure 13** shows the isotherm data, fitting results and the predicted isosteric heat of adsorption  $\Delta H_{ads}$  for each case. **Table 10** summarizes the values of Virial parameters, fitting statistics, and the heat of adsorption at infinite dilution  $\Delta H_{ads}^0$  (i.e. for very small CO<sub>2</sub> uptakes) calculated using equation (31) for the corresponding cases. We observe that case 1 with 2  $a_i$  and 1  $b_j$  parameters, fails to accurately fit the isotherm data, at both low and high CO<sub>2</sub> uptakes (**Figure 13a** left and middle). This leads to significant differences in HeatFit and GCMC predicted  $\Delta H_{ads}$  values (**Figure 13a** right).

In case 2, a better fit at low CO<sub>2</sub> uptakes was obtained using 3  $a_i$  and 2  $b_j$  parameters (**Figure 13b** middle) leading to a better agreement between GCMC and HeatFit predicted  $\Delta H_{ads}$  values. A close look at equation (29) suggests that the parameters  $a_0$  and  $b_0$  contribute to the Virial equation most for low uptake values, while the contribution from remaining parameters becomes significant at higher uptake values. Consequently, a good fit for low uptake values gives a much better estimation of  $a_0$  and  $b_0$  leading to a more accurate prediction of  $\Delta H_{ads}$  at low uptakes.

In case 3 (5  $a_i$  and 2  $b_j$  parameters) and case 4 (7  $a_i$  and 2  $b_j$  parameters) the fitting improved at higher CO<sub>2</sub> uptakes as well leading to an even better fit with and RMSE value of 0.2443, and 0.106, respectively. This suggests that an improved fit with lower RMSE values can always be obtained by using more Virial parameters. However, it is also important to check for the standard errors associated with the estimated parameter. **Table 10** shows that the standard errors associated with the estimated parameter values increase with the increasing number of parameters. Hence, while case 4 has the lowest RMSE value, the fitting parameters are unreliable because the standard errors for some parameters are of the same order as the corresponding parameter values (i.e  $a_3$  and  $a_4$  in case 4). It is worth mentioning here that the GUI features of HeatFit enable users to quickly try different numbers of Virial parameters for Virial equation fitting and check the RMSE value and the standard errors associated with the fitting results. We recommend that users of our program begin with a minimal number of parameters, gradually increasing the number of parameters while also keeping the check on standard errors and RMSE values until no significant

improvement in RMSE is observed and the standard errors are reasonable. In the case of Virial equation fitting with many parameters, we recommend using a ‘multi-start’ feature of HeatFit to find the best possible fitting results.

**Table 10.** Virial fitting results using various number of Virial parameters for CO<sub>2</sub> adsorption in CALF-20

Parameters	Case 1 $a_i = 2, b_j = 1$	Case 2 $a_i = 3, b_j = 2$	Case 3 $a_i = 5, b_j = 2$	Case 4 $a_i = 7, b_j = 2$	Units
$a_0$	$-5260.6 \pm 186.4$	$-4584.6 \pm 176.7$	$-4583.4 \pm 144.3$	$-4504.4 \pm 51.2$	K
$a_1$	$327.6 \pm 6.7$	$-239.7 \pm 71.6$	$-600.3 \pm 79.7$	$-170.0 \pm 48.4$	K mol <sup>-1</sup>
$a_2$	—	$41.6 \pm 2.75$	$347.8 \pm 44.3$	$-226.0 \pm 86.5$	K mol <sup>-2</sup>
$a_3$	—	—	$-75.2 \pm 12.7$	$72.8 \pm 64.4$	K mol <sup>-3</sup>
$a_4$	—	—	$5.87 \pm 1.2$	$38.6 \pm 22.3$	K mol <sup>-4</sup>
$a_5$	—	—	—	$-16.4 \pm 3.6$	K mol <sup>-4</sup>
$a_6$	—	—	—	$1.55 \pm 0.22$	K mol <sup>-5</sup>
$b_0$	$23.5 \pm 0.61$	$21.6 \pm 0.58$	$21.8 \pm 0.48$	$21.4 \pm 0.17$	—
$b_1$	—	$1.24 \pm 0.22$	$1.10 \pm 0.19$	$1.27 \pm 0.067$	—
$\Delta H_{ads}^0$	$-43.74 \pm 1.55$	$-38.12 \pm 1.46$	$-38.10 \pm 1.20$	$-37.45 \pm 0.42$	kJ mol <sup>-1</sup>
$r^2$	0.9884	0.9957	0.9972	0.9995	—
RMSE	0.4846	0.2978	0.2421	0.1060	—

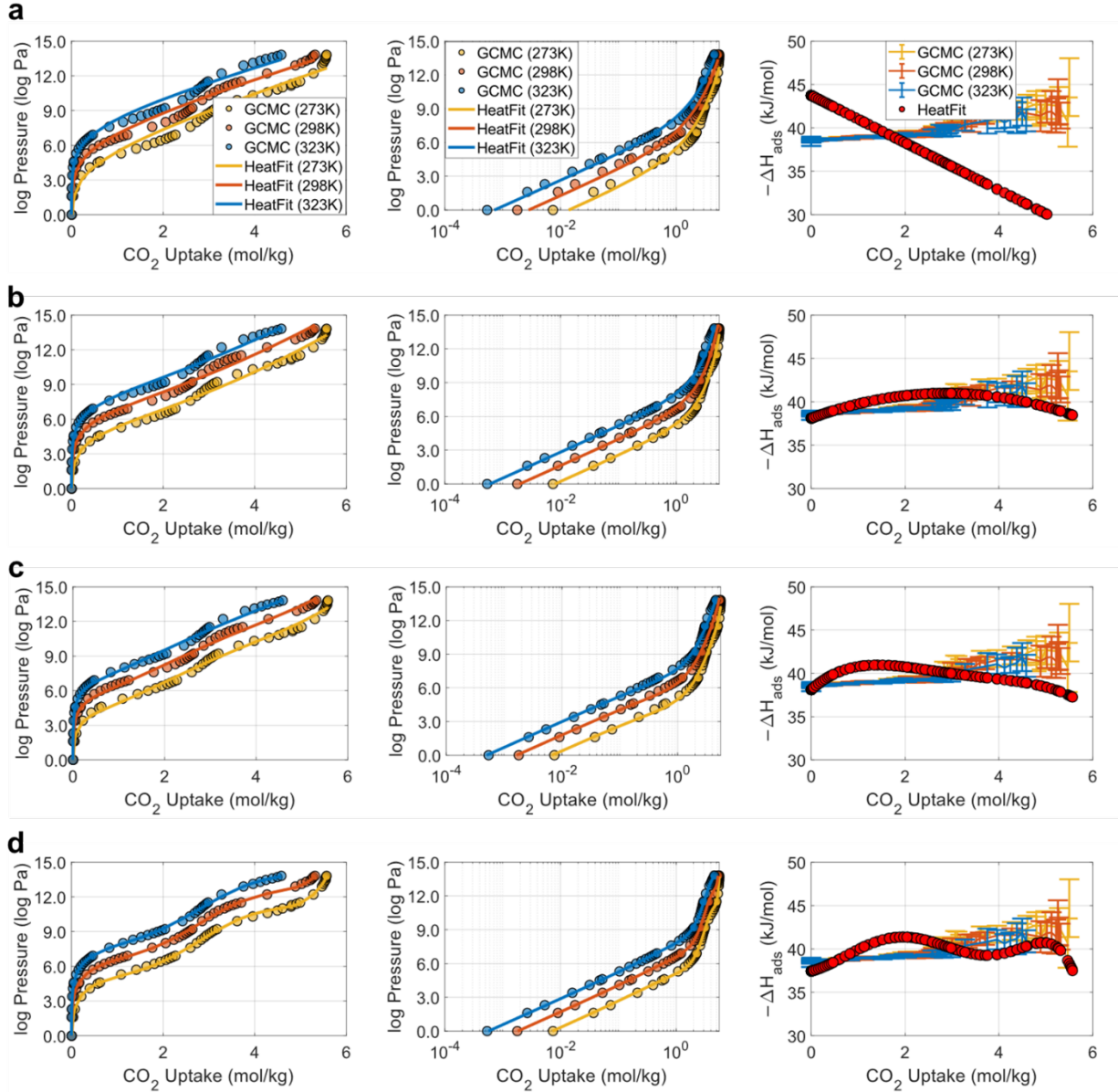


**Fig. 13.** Virial equation fitting results for CO<sub>2</sub> adsorption in CALF-20 using various number of Virial parameters. **a.** Fitting results with 2  $a_i$  and 1  $b_j$  parameters. **b.** Fitting results with 3  $a_i$  and 2  $b_j$  parameters. **c.** Fitting results with 5  $a_i$  and 2  $b_j$  parameters. **d.** Fitting results with 7  $a_i$  and 2  $b_j$  parameters. **Left.** Isotherm data and Virial fitting curves in  $\log p$  vs CO<sub>2</sub> uptake form. Filled circles and solid lines represent the CO<sub>2</sub> uptakes from GCMC simulation and Virial equation using HeatFit, respectively. **Middle.** Isotherm data and Virial fitting curves in  $\log p$  vs CO<sub>2</sub> uptake form with uptake scale in logarithmic form showing the fitting results at low CO<sub>2</sub> uptake values. **Right.** Isosteric heat of adsorption  $\Delta H_{ads}$  as a function of CO<sub>2</sub> uptake as obtained from GCMC simulation

and Virial equation using HeatFit. The solid lines with error bars and red filled circles correspond to  $\Delta H_{ads}$  values from GCMC and Virial equation, respectively

We also consider the uncertainty quantification of Virial equation parameters for the case with 5  $a_i$  and 2  $b_j$  parameters. **Figure 14** shows the probability distributions for Virial equation parameters and isosteric heat of adsorption at infinite dilution  $\Delta H_{ads}^0$ . The probability distributions for Virial equation parameters have been obtained from the Bayesian inference analysis discussed in **section 8.1** and **Appendix B**. The probability distribution of Virial parameter  $a_0$  have been propagated through equation (31) to obtain the distribution of  $\Delta H_{ads}^0$ . The multiple peaks in the parameter distributions reveal that multiple combinations of these Virial parameters can describe the isotherm data. In this case, it would be misleading to calculate and rely on point estimates like mean, however, the comparison can be made by comparing the peaks of probability distribution with the parameter values obtained from HeatFit since the height of the peaks in the probability distribution represents the likelihood of the parameter values from the isotherm data. The good agreement between the parameter values obtained from HeatFit and probability distribution peaks reveals that given the uncertainty in parameter values. The presence of multiple peaks with varying heights as well as breadth of probability distributions implies some degree of uncertainty in estimated parameters. We also observe that the uncertainty relative to parameter values is more pronounced for higher order Virial parameters (**Table 10**). For example, the parameters  $a_0$  and  $b_0$  contribute to the model most for low uptake values, while the remaining parameters contribute significantly to higher uptake values and inversely proportional to the temperature. Therefore, we recommend incorporating isotherm data with higher uptake values or isotherm data measured at lower temperatures to help capture the relative influence of higher order Virial parameters on model predictions and to get a better estimate of Virial parameters.

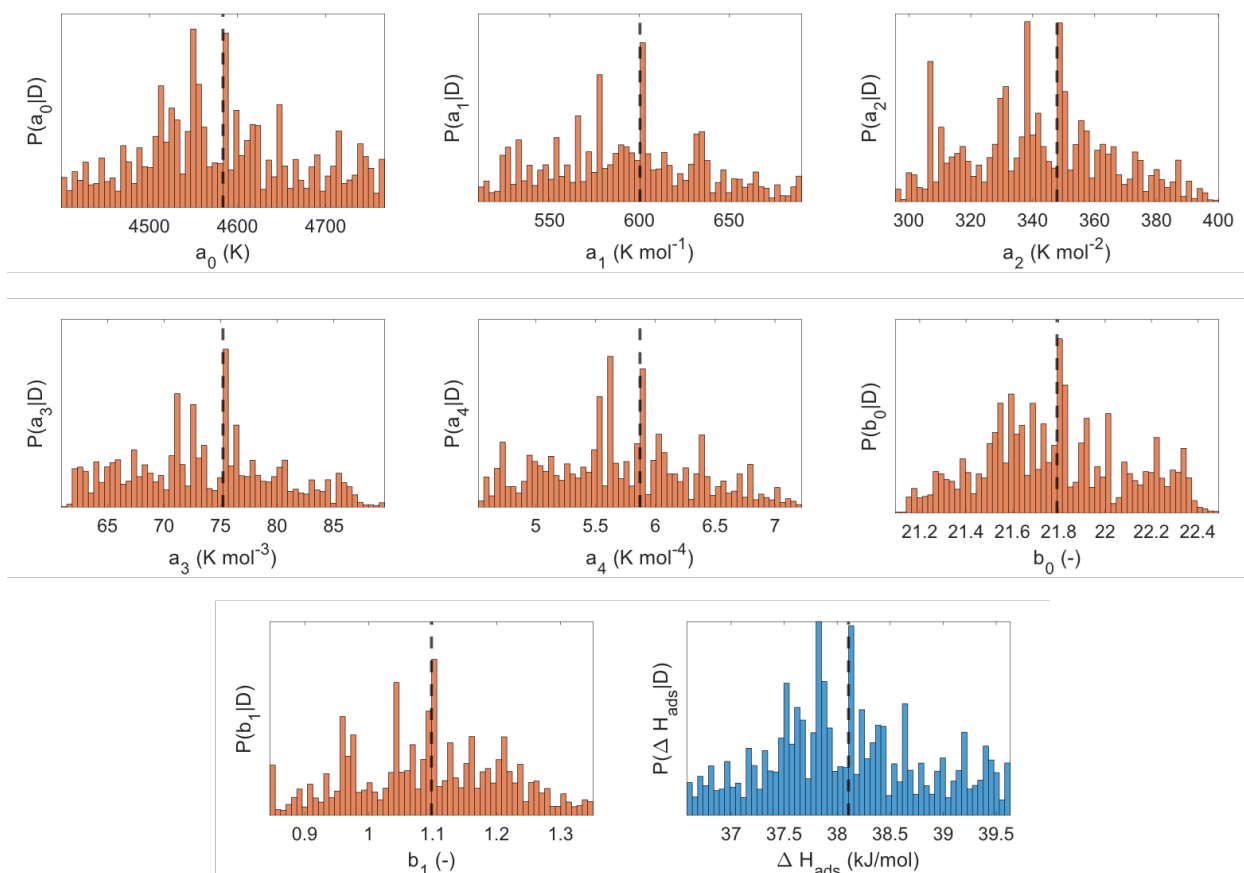


**Fig. 14.** Uncertainty quantification for the Virial equation parameters and infinite dilution isosteric heat of adsorption for CO<sub>2</sub> adsorption in CALF-20. The black dashed lines indicate the fitting values obtained from HeatFit.



#### 8.4. Non-isothermal breakthrough simulation using BreakLab

This section presents the case of non-isothermal breakthrough simulation of CO<sub>2</sub>/N<sub>2</sub> mixture using zeolite-13X. The isotherm parameters for CO<sub>2</sub> and N<sub>2</sub> adsorption in zeolite-13X have been obtained from Haghpanah *et al.* [59] and are tabulated in **Table 11**. The isotherm parameters correspond to dual and single-site Langmuir models for CO<sub>2</sub> and N<sub>2</sub>, respectively.

**Table 11.** Isotherm parameters for Zeolite 13X [59] used in the non-isothermal case study

Parameters	CO <sub>2</sub>	N <sub>2</sub>	Units
$q_{sat,1}$	3.09	5.84	mol kg <sup>-1</sup>
$b_1$	$9.24 \times 10^{-4}$	$5.94 \times 10^{-7}$	Pa <sup>-1</sup>
$\Delta U_{ads,1}$	-36.64	-15.80	kJ mol <sup>-1</sup>
$q_{sat,2}$	2.54	—	mol kg <sup>-1</sup>
$b_2$	$1.91 \times 10^{-5}$	—	Pa <sup>-1</sup>
$\Delta U_{ads,2}$	-35.69	—	kJ mol <sup>-1</sup>

**Table 12** lists the parameters used in the breakthrough simulation using BreakLab. The EDSL model has been used to evaluate the mixture adsorption loadings. The column is assumed to be initially filled with helium gas. The column is adiabatic, which means no heat transfer takes place to or from the column wall. In BreakLab, adiabatic condition can be imposed by specifying the heat transfer coefficient of the wall as zero. All process parameters were obtained from Haghpanah *et al.* [59], except for the mass transfer coefficients and isosteric heat of adsorption. In the model proposed by Haghpanah *et al.*, the mass transfer coefficients are a function of the adsorbed quantity and gas phase composition; hence, they are evaluated dynamically. BreakLab requires a constant mass transfer coefficient, and we used the mass transfer coefficients reported by Caballero *et al.* [63] for zeolite-13X under similar process conditions. Similarly, the BreakLab requires a single constant value of the isosteric heat of adsorption for each of the adsorbing components. We calculated the isosteric heat of adsorption using:

$$\Delta H_{ads,i} = \Delta U_{ads,i} - RT_{feed} \quad (63)$$

where  $\Delta U_{ads,i}$  is the internal energy change of adsorption for component  $i$ ,  $R$  is the general gas constant, and  $T_{feed}$  is the feed gas temperature in units of Kelvin.  $\Delta U_{ads}$  values for CO<sub>2</sub> and N<sub>2</sub> are listed in **Table 11**. Note that for CO<sub>2</sub>, we used the average value of  $\Delta U_{ads,1}$  and  $\Delta U_{ads,2}$ .

**Table 12.** Properties and parameters [59] used in the non-isothermal adsorption breakthrough simulation case study

Parameters		Value	Units
<i>Feed gas</i>			
Temperature		25	°C
Specific heat capacity		30.7	J mol <sup>-1</sup> K <sup>-1</sup>
Thermal conductivity		0.09	W m <sup>-1</sup> K <sup>-1</sup>
Molecular diffusivity		$1.60 \times 10^{-5}$	m <sup>2</sup> s <sup>-1</sup>
Gas viscosity		$1.72 \times 10^{-5}$	kg m <sup>-1</sup> s <sup>-1</sup>
Feed velocity		0.37	m s <sup>-1</sup>
Composition (mole fraction)	CO <sub>2</sub>	0.15	—
	N <sub>2</sub>	0.85	—
Mass transfer coefficient	CO <sub>2</sub>	0.1631	s <sup>-1</sup>
	N <sub>2</sub>	0.2044	s <sup>-1</sup>
Isosteric heat of adsorption	CO <sub>2</sub>	-38.64	kJ mol <sup>-1</sup>
	N <sub>2</sub>	-18.28	kJ mol <sup>-1</sup>
<i>Adsorber column</i>			
Pressure		100	kPa
Length		1.0	m
Diameter		0.289	m
Wall Temperature		25	°C
Inside wall heat transfer coefficient		0	W m <sup>-2</sup> K <sup>-1</sup>
Solid bulk density		711	kg m <sup>-3</sup>
Particle diameter		$2 \times 10^{-3}$	m
Particle porosity		0.35	—
Bed porosity		0.37	—
Solid specific heat capacity		1070	J kg <sup>-1</sup> K <sup>-1</sup>

**Figure 15** shows the composition and temperature breakthrough profiles obtained from the BreakLab module. The composition breakthrough profiles (**Figure 15a**) reveal the instantaneous breakthrough of N<sub>2</sub>. The CO<sub>2</sub> breakthrough curve shows two characteristic fronts. First, a sharp increase in CO<sub>2</sub> composition represents the CO<sub>2</sub> compositional front breakthrough. The second relatively small and diffused increase in CO<sub>2</sub> composition is due to the thermal front [59]. **Figure 15b** shows the corresponding temperature breakthrough profile, where the gas temperature initially increases rapidly due to CO<sub>2</sub> breakthrough and then returns to the feed temperature after the thermal front exits the column.

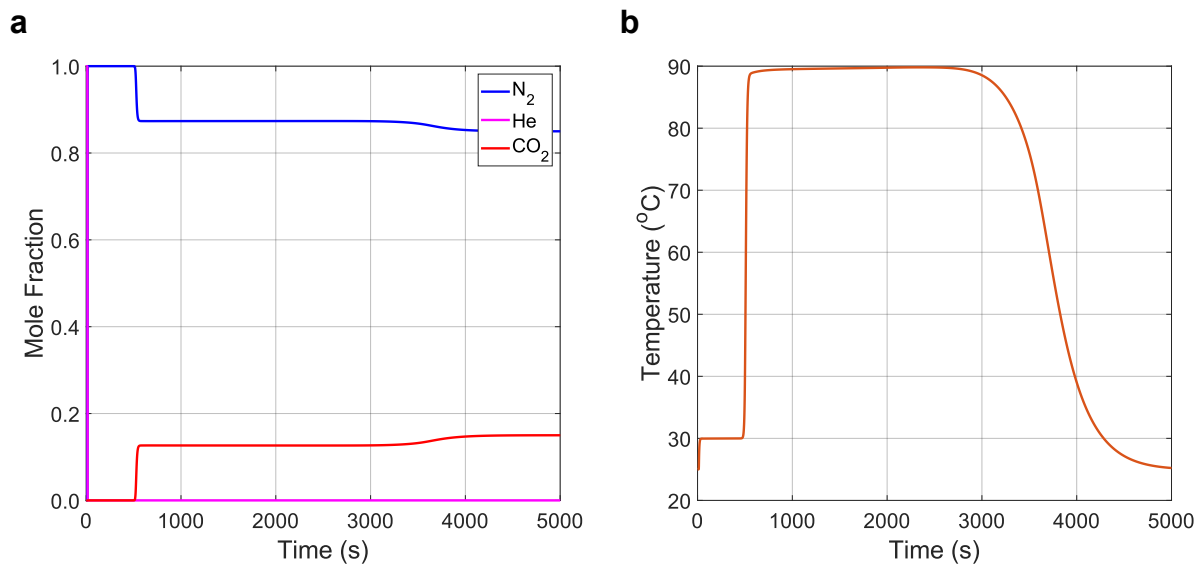


**Fig. 15.** Breakthrough curves for CO<sub>2</sub> and N<sub>2</sub> adsorption in zeolite 13X obtained from BreakLab.  
**a.** Composition breakthrough curve **b.** Temperature breakthrough curve at the outlet of the adsorber column

## 9. Conclusions

AIM is a MATLAB-based GUI workflow software designed to streamline the analysis of adsorbent materials through an integrated computational workflow encompassing isotherm fitting, isosteric heat of adsorption estimation, mixture isotherm prediction, and multicomponent breakthrough simulations. The four modules – IsoFit, HeatFit, MixPred, and BreakLab – offer a user-friendly GUI that supports a wide range of isotherm models (e.g., Langmuir, BET, Toth) and advanced simulation capabilities, such as non-isothermal breakthrough analysis with axial dispersion and Linear Driving Force (LDF) mass transfer. Case studies including Xe/Kr separation in SBMOF-1, CO<sub>2</sub>/CH<sub>4</sub> separation in CALF-20, and CO<sub>2</sub>/N<sub>2</sub> adsorption in zeolite 13X, demonstrate AIM's functionality and versatility, with results closely matching existing tools such as RUPTURA. By providing open-source access to the GUI via GitHub, we aim to promote reproducibility and accessibility in adsorption science and engineering for both experimentalists and computational researchers. However, limitations such as the reliance of constant mass transfer coefficients in BreakLab and challenges in fitting higher-order Virial parameters highlight areas for future refinement and improvement. Future work will focus on incorporating dynamic mass transfer models, expanding available isotherm libraries, and integrating physical properties libraries of different gas components.

## **Author Information**

### **Corresponding Author**

Yongchul G. Chung – *School of Chemical Engineering, Pusan National University, Busan 46241, Republic of Korea.*

Email: [drygchung@gmail.com](mailto:drygchung@gmail.com)

### **Authors**

Muhammad Hassan – *School of Chemical Engineering, Pusan National University, Busan 46241, Republic of Korea.*

Sunghyun Yoon – *School of Chemical Engineering, Pusan National University, Busan 46241, Republic of Korea.*

Yu Chen – *School of Chemical Engineering, Pusan National University, Busan 46241, Republic of Korea.*

Pilseok Kim – *Department of Chemical and Biological Engineering, Korea University, 145 Anam-ro, Seongbuk-gu, Seoul 02841, Republic of Korea*

Hongryeol Yun – *Department of Chemistry, Korea University, Seoul 02841, Republic of Korea*

Youn-Sang Bae – *Department of Chemical and Biomolecular Engineering, Yonsei University, 50 Yonsei-ro, Seodaemun-gu, Seoul, 03722, Republic of Korea.*

Chung-Yul Yoo – *Department of Energy Systems Research and Chemistry, Ajou University, 206, World Cup-ro, Yeongtong-gu, Suwon 16499, Republic of Korea.*

Dong-Yeun Koh – *Department of Chemical and Biomolecular Engineering (BK-21 Plus), Korea Advanced Institute of Science and Technology (KAIST), Daejeon 34141, Republic of Korea.*

Chang-Seop Hong – *Department of Chemistry, Korea University, Seoul 02841, Republic of Korea*

Ki-Bong Lee – *Department of Chemical and Biological Engineering, Korea University, 145 Anam-ro, Seongbuk-gu, Seoul 02841, Republic of Korea*

Yongchul G. Chung – *School of Chemical Engineering, Graduate School of Data Science Pusan National University, Busan 46241, Republic of Korea.*

### **Author Contributions**

**Muhammad Hassan:** Conceptualization, Data curation, Methodology, Formal analysis, Software, Visualization, Writing – original draft, Writing – review and editing. **Sunghyun Yoon:** Methodology, Data curation, Visualization, Writing – review and editing. **Yu Chen:** Data curation. **Pilseok Kim:** Validation, Writing – review. **Hongryeol Yun:** Validation, Writing – review. **Hyuk Take Kwon:** Validation, Writing – review. **Youn-Sang Bae:** Validation, Writing – review. **Chung-Yul Yoo:** Validation, Writing – review. **Dong-Yeun Koh:** Validation, Writing – review. **Chang-Seop Hong:** Validation, Writing – review. **Ki-Bong Lee:** Validation, Writing – review. **Yongchul G. Chung:** Conceptualization, Supervision, Resources, Project administration, Funding acquisition, Writing – review and editing.

### **Acknowledgements**

This work was supported by the National Research Foundation of Korea (NRF) from a grant funded by the Korea government (MSIT) (RS-2024-00449431).

### **Declaration of Competing Interest**

The authors declare that they have no conflict of interest.

### **Data Availability**

The data and MATLAB code to reproduce the figures in the manuscript can be found at AIM GitHub repository (<https://github.com/mtap-research/AIM>).

## Appendix A. Molecular simulation

The grand canonical Monte Carlo (GCMC) simulations were conducted to predict the single component adsorption data for CO<sub>2</sub>/CH<sub>4</sub> in CALF-20 and Xe/Kr in SBMOF-1 with a range of pressure (1 Pa up to 1,000,000 Pa) at 298K. Each GCMC simulation consisted of 20,000 cycles, where the initial 10,000 cycles were used for initialization, and the remaining 10,000 cycles were used for the ensemble averages. The swap (insertion and deletion) translation, rotation, and reinsertion Monte Carlo (MC) move were applied for MC sampling with equal probabilities.

The Lennard-Jones 12-6 potential was used to model the non-bonded interaction between zeolites and gases. The TraPPE forcefield [68] was used for CO<sub>2</sub>/CH<sub>4</sub>, and the UFF [69] was used to model the Xe/Kr molecule. Dreiding force field [70] was employed for the frameworks. The Lorentz-Berthelot mixing rules were used to calculate the LJ parameters for different atom-type interaction. The van der Waals interactions among atoms in the system were truncated at 14.0 Å with an analytic tail correction. All MC and GCMC simulations were carried out using RASPA 2.0 [71].



## Appendix B. Bayesian inference for uncertainty quantification

The parameters obtained from fitting adsorption isotherm data inherently carry a degree of uncertainty. This uncertainty arises from both measurement uncertainties in the isotherm data and potential limitations of the isotherm model itself. Given that isotherm models are widely used for predicting mixture adsorption and simulating breakthrough behavior, any uncertainty in the model parameters directly impacts the reliability and accuracy of these predictions. Therefore, quantifying the uncertainties associated with isotherm model parameters is essential to ensure the robustness of model predictions. In this study, we employed the uncertainty quantification framework proposed by Ward *et al.* [67], utilizing Bayesian inference analysis for isotherm fitting. Bayesian inference analysis is a well-known tool for the quantification of uncertainties in model parameters given the measured data. In Bayesian inference the model parameters are represented as probability distributions. The mean value of these parameter probability distributions corresponds to the point estimate of the parameter value which would be obtained from traditional model fitting. Additionally, the width of such probability distributions represents the degree of uncertainty in the estimated parameter value. Bayesian inference analysis updates our existing knowledge about model parameters by incorporating the new information obtained from the measured data.

The Bayesian update is based on the Baye's theorem:

$$P(\boldsymbol{\theta}|\mathcal{D}) = \frac{P(\mathcal{D}|\boldsymbol{\theta}) P(\boldsymbol{\theta})}{P(\mathcal{D})} \quad (\text{B.1})$$

where  $\boldsymbol{\theta} = (\theta_1, \theta_2, \theta_3, \dots, \theta_N)$  are the model parameters,  $P(\boldsymbol{\theta})$  is the existing or prior distribution of the model parameters,  $\mathcal{D}$  is the set of measured data,  $P(\mathcal{D}|\boldsymbol{\theta})$  is the likelihood function and represent the probability of data given the model parameters.  $P(\boldsymbol{\theta}|\mathcal{D})$  is the probability of model parameters given the measured data also called posterior distribution. The posterior distribution  $P(\boldsymbol{\theta}|\mathcal{D})$  represents how likely the model parameters are given the measured data. The term  $P(\mathcal{D})$  is the normalizing constant which ensures that the cumulative area under the posterior distribution is unity. A detailed description of calculating the likelihood function, normalizing constant and prior probability distribution has been provided by Ward *et al.* [67]. Here we only present the resulting expressions.

For the expression of the likelihood function, the errors between the measured data and model predictions for the given set of parameters are assumed to be normally distributed. This assumption yields the following expression for likelihood function:

$$P(\mathcal{D}|\boldsymbol{\theta}) = \frac{1}{(\sqrt{2\pi} \sigma)^{N_p}} \exp \left[ -\frac{\sum_{i=1}^{N_p} (Q_i^{exp} - Q_i^{sim})^2}{2\sigma^2} \right] \quad (\text{B.2})$$

where  $N_p$  is the number of measurements in the data  $\mathcal{D}$ . The terms  $Q_i^{exp}$  and  $Q_i^{sim}$  are the values of the  $i^{th}$  measurement and the corresponding model prediction for the given model parameters  $\boldsymbol{\theta}$ , respectively. The term  $\sigma$  is the standard deviation of the error between the data and the model. From the definition of likelihood function, it follows that the  $P(\mathcal{D}|\boldsymbol{\theta})$  is high for the model parameters which results in smaller values of residual error.

The expression for the prior probability distribution is derived from the maximum entropy principle and is given as,

$$P(\theta_j) = \frac{1}{\theta_{j,nom}} \exp \left[ -\frac{\theta_j}{\theta_{j,nom}} \right] \quad (\text{B.3})$$

where  $\theta_{j,nom}$  is the nominal or fitted value of the  $j^{th}$  model parameter  $\theta_j$ . Equation (B.3) is the marginal prior distribution depending only on the given parameter  $\theta_j$ . Assuming that all the model parameters are independent of one another, a joint prior probability distribution considering all the model parameters  $\boldsymbol{\theta} = (\theta_1, \theta_2, \theta_3, \dots, \theta_N)$  can be obtained as follows,

$$P(\boldsymbol{\theta}) = \prod_{j=1}^{n_p} \left( \frac{1}{\theta_{j,nom}} \exp \left[ -\frac{\theta_j}{\theta_{j,nom}} \right] \right) \quad (\text{B.4})$$

where  $n_p$  is the total number of model parameters.

The normalizing constant  $P(\mathcal{D})$  is obtained by integrating the joint probability distributions of the data given the model parameters  $P(\mathcal{D}|\boldsymbol{\theta})$  and prior probability of model parameters  $P(\boldsymbol{\theta})$  over the full domain of model parameters.

$$P(\mathcal{D}) = \int_{\theta} P(\mathcal{D}|\theta) P(\theta) d\theta \quad (\text{B.5})$$

Using equations (B.2), (B.4), and (B.5), we can determine the joint posterior distribution  $P(\theta|\mathcal{D})$ . The marginal probability distribution for each of the model parameters can be obtained by marginalizing equation (B1) that is,

$$P(\theta_j|\mathcal{D}) = \int_{\theta_{-j}} \frac{P(\mathcal{D}|\theta) P(\theta)}{P(\mathcal{D})} d\theta_{-j} \quad (\text{B.6})$$

where  $\theta_{-j}$  represents that integral is taken with respect to all the model parameters except  $\theta_j$ .

Together equations (B.2-B.6) constitute Bayesian inference for obtaining posterior probability distribution of model parameters. The integrals in equations (B.5) and (B.6) are multidimensional and are evaluated using Monte Carlo integration techniques. A MATLAB based implementation of Bayesian inference using quasi-Monte Carlo integration has been provided by Ward *et al.* [67]. We used the supplied code and coupled it with our isotherm functions to obtain uncertainty in the model parameters for the case studies.

## REFERENCES

- [1] D.M. Ruthven, Principles of Adsorption and Adsorption Processes, John Wiley & Sons, Inc., 1984.
- [2] J.D. Seader, E.J. Henley, D.K. Roper, Separation Process Principles- Chemical and Biochemical Operations, 3rd ed., John Wiley & Sons, Inc., 2011.
- [3] K.T. Leperi, Y.G. Chung, F. You, R.Q. Snurr, ACS Sustain Chem Eng 7 (2019) 11529–11539.
- [4] A.K. Rajagopalan, A.M. Avila, A. Rajendran, International Journal of Greenhouse Gas Control 46 (2016) 76–85.
- [5] J. Park, H.O. Rubiera Landa, Y. Kawajiri, M.J. Realff, R.P. Lively, D.S. Sholl, Ind Eng Chem Res 59 (2020) 7097–7108.
- [6] A. Rajendran, S.G. Subraveti, K.N. Pai, V. Prasad, Z. Li, Acc Chem Res 56 (2023) 2354–2365.
- [7] A.H. Farmahini, S. Krishnamurthy, D. Friedrich, S. Brandani, L. Sarkisov, Chem Rev 121 (2021) 10666–10741.
- [8] I. van Zandvoort, E.J. Ras, R. de Graaf, R. Krishna, Sep Purif Technol 241 (2020) 116706.
- [9] Q. Hu, Y. Xie, Z. Zhang, Sep Purif Technol 238 (2020) 116399.
- [10] D. Bahamon, L.F. Vega, Chemical Engineering Journal 284 (2016) 438–447.
- [11] S. Xiang, Y. He, Z. Zhang, H. Wu, W. Zhou, R. Krishna, B. Chen, Nature Communications 2012 3:1 3 (2012) 1–9.
- [12] R. Krishna, RSC Adv 5 (2015) 52269–52295.
- [13] A.P. Ladshaw, A.I. Wiechert, A.K. Welty, K.L. Lyon, J.D. Law, R.T. Jubin, C. Tsouris, S. Yiacoumi, Chemical Engineering Journal 375 (2019) 122073.
- [14] Y.G. Chung, P. Bai, M. Haranczyk, K.T. Leperi, P. Li, H. Zhang, T.C. Wang, T. Duerinck, F. You, J.T. Hupp, O.K. Farha, J.I. Siepmann, R.Q. Snurr, Chemistry of Materials 29 (2017) 6315–6328.
- [15] X. Cui, K. Chen, H. Xing, Q. Yang, R. Krishna, Z. Bao, H. Wu, W. Zhou, X. Dong, Y. Han, B. Li, Q. Ren, M.J. Zaworotko, B. Chen, Science (1979) 353 (2016) 141–144.
- [16] R. Krishna, J.R. Long, Journal of Physical Chemistry C 115 (2011) 12941–12950.
- [17] R. Krishna, RSC Adv 7 (2017) 35724–35737.
- [18] A.L. Myers, J.M. Prausnitz, AIChE Journal 11 (1965) 121–127.
- [19] R. Krishna, ACS Omega 5 (2020) 16987–17004.
- [20] J.M.P.Q. Delgado, Heat and Mass Transfer/Waerme- Und Stoffuebertragung 42 (2006) 279–310.
- [21] S. Sircar, Sep Purif Technol 192 (2018) 383–400.
- [22] S. Ga, Y.G. Chung, Mol Syst Des Eng 7 (2022) 686–701.
- [23] C.M. Simon, B. Smit, M. Haranczyk, Comput Phys Commun 200 (2016) 364–380.
- [24] S. Lee, J.H. Lee, J. Kim, Korean Journal of Chemical Engineering 35 (2018) 214–221.
- [25] P. Iacomini, P.L. Llewellyn, Adsorption 25 (2019) 1533–1542.
- [26] S. Sharma, S.R.G. Balestra, R. Baur, U. Agarwal, E. Zuidema, M.S. Rigutto, S. Calero, T.J.H. Vlucht, D. Dubbeldam, Mol Simul 49 (2023) 893–953.
- [27] S. Ga, N. An, C. Joo, J. Kim, Comput Phys Commun 291 (2023) 108830.
- [28] T. Kim, J.K. Scott, Comput Chem Eng 176 (2023) 108309.

- [29] J.D. Evans, V. Bon, I. Senkovska, S. Kaskel, *Langmuir* 37 (2021) 4222–4226.
- [30] I. Langmuir, *J Am Chem Soc* 40 (1918) 1361–1403.
- [31] D. Graham, *J Phys Chem* 57 (1953) 665–669.
- [32] R. Sips, *J Chem Phys* 16 (1948) 490–495.
- [33] R.A. Koble, T.E. Corrigan, *Ind Eng Chem* 44 (1952) 383–387.
- [34] G.A. Guiochon, A. Felinger, A. Katti, D.G. Shirazi, *Fundamentals of Preparative and Nonlinear Chromatography*, Elsevier, Amsterdam, Netherlands, 2006.
- [35] B. Lin, Z. Ma, S. Golshan-Shirazi, G. Guiochon, *J Chromatogr A* 475 (1989) 1–11.
- [36] A. Tarafder, M. Mazzotti, *Chem Eng Technol* 35 (2012) 102–108.
- [37] C.M. Simon, J. Kim, L.-C. Lin, R.L. Martin, M. Haranczyk, B. Smit, *Physical Chemistry Chemical Physics* 16 (2014) 5499–5513.
- [38] S. Brunauer, P.H. Emmett, E. Teller, *J Am Chem Soc* 60 (1938) 309–319.
- [39] Do D., *Adsorption Analysis: Equilibria and Kinetics*, Imperial College Press, 1998.
- [40] J. TOTH, *Acta Chim. Hung.* 69 (1971) 311–328.
- [41] J. Tóth, *Adv Colloid Interface Sci* 55 (1995) 1–239.
- [42] S. Hiraide, Y. Sakanaka, Y. Iida, H. Arima, M.T. Miyahara, S. Watanabe, *Proc Natl Acad Sci U S A* 120 (2023) e2305573120.
- [43] M.M. Dubinin, V.A. Astakhov, *Bulletin of the Academy of Sciences of the USSR Division of Chemical Science* 20 (1971) 8–12.
- [44] M.M. DUBININ, 9 (1975) 1–70.
- [45] V.J. Inglezakis, S.G. Pouloupoulos, H. Kazemian, *Microporous and Mesoporous Materials* 272 (2018) 166–176.
- [46] I.M. Klotz, F.M. Walker, R.B. Pivan, *J Am Chem Soc* 68 (1946) 1486–1490.
- [47] C. Buttersack, *Physical Chemistry Chemical Physics* 21 (2019) 5614–5626.
- [48] M. Thommes, K. Kaneko, A. V. Neimark, J.P. Olivier, F. Rodriguez-Reinoso, J. Rouquerol, K.S.W. Sing, *Pure and Applied Chemistry* 87 (2015) 1051–1069.
- [49] D.D. Do, H.D. Do, *Carbon N Y* 38 (2000) 767–773.
- [50] D.D. Do, S. Junpirom, H.D. Do, *Carbon N Y* 47 (2009) 1466–1473.
- [51] H. Pan, J.A. Ritter, P.B. Balbuena, *Langmuir* 14 (1998) 6323–6327.
- [52] A. Nuhnen, C. Janiak, *Dalton Transactions* 49 (2020) 10295–10307.
- [53] L. Czepirski, J. JagieŁŁo, *Chem Eng Sci* 44 (1989) 797–801.
- [54] J.A. V. Butler, C. Ockrent, *J Phys Chem* 34 (1930) 2841–2859.
- [55] A.H. Farmahini, S. Krishnamurthy, D. Friedrich, S. Brandani, L. Sarkisov, *Ind Eng Chem Res* 57 (2018) 15491–15511.
- [56] A.L. Myers, *AIChE Journal* 29 (1983) 691–693.
- [57] A.L. Myers, P.A. Monson, *Adsorption* 20 (2014) 591–622.
- [58] E. Mangano, D. Friedrich, S. Brandani, *AIChE Journal* 61 (2015) 981–991.
- [59] R. Haghighpanah, A. Majumder, R. Nilam, A. Rajendran, S. Farooq, I.A. Karimi, M. Amanullah, *Ind Eng Chem Res* 52 (2013) 4249–4265.
- [60] A. Arora, S.S. Iyer, M.M.F. Hasan, *Chem Eng Sci* 192 (2018) 335–358.
- [61] The MathWorks Inc., (2024).
- [62] K.T. Leperi, R.Q. Snurr, F. You, (2015).
- [63] D. Yancy-Caballero, K.T. Leperi, B.J. Bucior, R.K. Richardson, T. Islamoglu, O.K. Farha, F. You, R.Q. Snurr, *Mol Syst Des Eng* 5 (2020) 1205–1218.
- [64] R. Eymard, T. Gallouët, R. Herbin, *Handbook of Numerical Analysis* 7 (2000) 713–1018.

- [65] X.-D. Liu, S. Osher, T. Chan, *J Comput Phys* 115 (1994) 200–212.
- [66] L.F. Shampine, M.W. Reichelt, *SIAM Journal on Scientific Computing* 18 (1997) 1–22.
- [67] A. Ward, R. Pini, *Adsorption* 28 (2022) 161–183.
- [68] C.G. Aimoli, E.J. Maginn, C.R.A. Abreu, *Fluid Phase Equilib* 368 (2014) 80–90.
- [69] A.K. Rappe, C.J. Casewit, K.S. Colwell, W.A. Goddard, W.M. Skiff, *J Am Chem Soc* 114 (1992) 10024–10035.
- [70] S.L. Mayo, B.D. Olafson, W.A. Goddard, *J Phys Chem* 94 (1990) 8897–8909.
- [71] D. Dubbeldam, S. Calero, D.E. Ellis, R.Q. Snurr, *Mol Simul* 42 (2016) 81–101.